Politecnico di Torino

Master's Degree in Energy and Nuclear Engineering

A.Y. 2025/2026

July 2026

Integration of Calcium Oxide based Thermochemical Storage in CSP Plants for Dispatchable Renewable Energy Supply

Relatori:

- **Prof.ssa Elisa Guelpa**
- **Prof. Ricardo Chacartegui**

Candidato:

- **Pietro Robaldo**

Ringraziamenti

Giunto al termine di questo percorso accademico, desidero esprimere la mia profonda gratitudine a tutte le persone che mi hanno supportato e accompagnato in questo cammino.

Il ringraziamento più grande va alla mia famiglia, che con il suo sostegno incondizionato mi ha permesso di affrontare con determinazione un percorso impegnativo come quello dell'Ingegneria, anche nei mesi trascorsi lontano da casa. Un grazie speciale a mia mamma, la cui vicinanza costante è stata per me fonte di forza e motivazione in ogni momento di questo cammino: a lei dedico questo traguardo.

Un grazie sentito va ai miei amici, quelli di sempre e quelli incontrati lungo il percorso, che con la loro presenza hanno reso più leggere le giornate di studio. I momenti di svago e di condivisione trascorsi insieme sono stati indispensabili per affrontare con equilibrio le sfide di questi anni.

Un sincero ringraziamento va alla Prof.ssa Elisa Guelpa, che mi ha offerto la possibilità di svolgere il lavoro di tesi presso l'Universidad de Sevilla. Senza la sua disponibilità e la sua fiducia, questa esperienza, che si è rivelata preziosa tanto sul piano accademico quanto su quello personale, non sarebbe stata possibile.

Desidero ringraziare il Prof. Ricardo Chacartegui, che mi ha seguito come relatore durante il periodo a Siviglia. La sua guida, la sua competenza e i suoi consigli sono stati fondamentali per la realizzazione di questa tesi, permettendomi di affrontare tematiche complesse con metodo e spirito critico.

Infine, un pensiero di gratitudine va ai professori del Politecnico di Torino, che con il loro insegnamento mi hanno trasmesso un metodo di studio rigoroso e mi hanno aiutato a sviluppare consapevolezza sulle mie passioni e sulle competenze che desidero coltivare nel mio futuro professionale.

Table of Contents

Table of figures

ABSTRACT

The transition toward a fully renewable energy system requires not only clean generation but also the ability to store energy and deliver it on demand, overcoming the mismatch between the intermittent availability of renewable sources and the continuous needs of the end users. Within this context, the objective of this thesis is to design and analyse an integrated solar plant able to supply electricity, heating, and cooling to a residential district located in the area of Seville, in southern Spain, entirely from solar energy and in a fully dispatchable way.

The proposed plant is a polygeneration system built around three sections operating in synergy. The first is a concentrated solar power (CSP) plant of the central-receiver type, in which a field of heliostats concentrates direct solar radiation onto a tower-mounted receiver to produce high-temperature heat. The second is a thermochemical energy storage based on the reversible $CaO/Ca(OH)_2$ hydration–dehydration reaction, which stores the collected solar energy in the form of chemical potential: during charging the solar heat dehydrates the calcium hydroxide, while during discharging the hydration of calcium oxide releases high-grade heat. The third is a trigeneration block, which converts the available thermal energy into the three energy services demanded by the district. The role of the storage is to decouple the delivery of energy from the availability of the sun, allowing the plant to follow the user demand continuously, including at night and during periods of low solar irradiance. Because the energy is stored as a chemically stable solid at ambient temperature, the system avoids the standby losses of conventional molten-salt thermal storage, providing a compact, safe and fully renewable supply of power, heat and cold.

The plant was sized to serve13,000 dwellings and was modelled through thermodynamic mass and energy balances, a daily-resolved annual energy model, and process simulation in DWSIM. The reference design comprises a 256,884 m^2 heliostat field feeding a 115.3 MWth central receiver, and a thermochemical storage capacity exceeding 3 GWhth. Two storage strategies were evaluated: a quasi-autonomous configuration with five days of autonomy and a grid-assisted configuration with two days of capacity. The operational simulations show that the system can satisfy nearly all of the annual district energy demand from solar resources, requiring only 6.4 GWh of winter electricity imports. A key finding is that the addition of a second 10 MWe condensing turbine allows the recovery of the excess summer solar energy, reducing the annual curtailment by 96% and exporting 43.6 GWh of renewable electricity to the grid.

The techno-economic analysis identifies this dual-turbine configuration as the most attractive solution, with a net present value of approximately 80 M€ over the 30-year lifetime, a discounted payback of sixteen years and a levelised cost of energy of 87 €/MWh. The study concludes that $CaO/Ca(OH)_2$ thermochemical storage represents a promising pathway for long-duration, high-temperature energy storage, enabling CSP-based systems to provide reliable, dispatchable and economically competitive multi-energy services at district scale.

1) INTRODUCTION

Purpose of energy storage systems

The transition toward a sustainable energy paradigm is undoubtedly the most ambitious technological and social challenge of our century. The progressive shift away from fossil fuels in favour of renewable sources, such as solar and wind power, has radically transformed the global power generation landscape. However, the enthusiasm for the growing installed capacity of these "green" sources must now be measured against a structural physical limit: their inherent intermittent nature.
Unlike traditional thermoelectric power plants, whose output can be modulated according to demand, renewable sources depend on unpredictable meteorological variables and natural cycles. This creates an energy paradox: overproduction during peak solar or wind hours cannot be exploited unless used instantaneously, risking energy curtailment, while during periods of stagnation, the grid remains vulnerable or forced to rely on fossil-based backup sources.
In this context, the stability of the future power grid will not depend solely on how much energy we can produce, but on how we are able to store it. The development of efficient, scalable, and environmentally low-impact Energy Storage systems has thus become the key element required to turn the ecological transition into a concrete and reliable reality. Current requirements do not only concern the need to store energy for short periods (a few hours) but also the capacity to manage medium- and long-duration storage (days or weeks), capable of ensuring energy security even during prolonged adverse weather scenarios. It is precisely within this technological gap that thermochemical energy storage systems like the calcium loop energy storage subject of this study find place, promising to overcome the energy density and temporal degradation limits typical of current storage technologies based on heat preservation.
The fundamental objective of energy storage technologies is to bridge the structural gap between generation and consumption curve. The primary goal is to enable renewable sources to cover the entire energy demand of end-users, effectively decoupling it from fossil fuel dependency. This milestone must be achieved despite the inherent asymmetry between the production curve, dictated by the natural availability of the resource, and the user demand curve, which follows often opposing social and industrial dynamics.

1.1) The energy context: renewables, CSP and storage

Before focusing on the specific technology developed in this work, it is useful to frame the three domains on which the proposed plant builds: the growth of solar energy and the role of concentrated solar power within it, the current landscape of energy-storage technologies, and the field of solar-based cogeneration and district energy. This context clarifies where the opportunity addressed by this thesis lies.

1.1.1) Solar energy and concentrated solar power

Solar energy has become the fastest-growing source of electricity in the world. Global cumulative solar capacity crossed the 1 TW mark in 2022 and reached roughly 2 TW by the end of 2024, adding close to 600 GW in that single year. The overwhelming majority of this capacity is photovoltaic (PV): concentrated solar power (CSP), which uses mirrors to concentrate sunlight and generate high-temperature heat, remains a niche technology, with about 6.9–7.2 GW installed worldwide in 2024. Most of the operating CSP fleet is located in Spain and the United States, the early lead markets, while recent growth is driven almost entirely by China, where a series of large "CSP+" projects co-locate 100 MW-class solar towers with hundreds of megawatts of PV and wind.

Despite its small share, CSP occupies a distinctive and strategic position. Unlike PV, which produces electricity directly and instantaneously, CSP generates heat that can be stored inexpensively before conversion, so that a CSP plant can be equipped with thermal storage and dispatch power on demand, including after sunset. This makes CSP a naturally dispatchable renewable technology, complementary to the variable output of PV, and particularly suited to regions with high direct normal irradiance such as southern Spain, the Middle East, North Africa and the American Southwest. It is precisely this ability to deliver high-temperature heat that makes CSP the ideal primary source for a thermochemical storage system.

1.1.2) Energy-storage technologies

The dispatchability that CSP offers depends on the storage technology coupled to it, and more broadly the whole energy transition hinges on the availability of adequate storage. The current landscape is dominated by two families. Electrochemical batteries, above all lithium-ion, excel at short-duration, fast-response applications and have seen dramatic cost reductions, but they rely on scarce and critical materials, have a limited lifespan and present safety concerns, which make them ill-suited to large-scale storage over days or weeks. Thermal storage, in the form of two-tank molten salts, is the established solution in the CSP sector and provides typically 8 to 15 hours of autonomy, but it stores energy as sensible heat and therefore suffers continuous thermal losses through the tank walls, which rules it out for long-duration or seasonal storage.

Between the short-duration strengths of batteries and the medium-duration role of molten salts, a gap remains for technologies able to store large amounts of energy over days or seasons without degradation. Thermochemical energy storage (TCES), which stores energy in the chemical bonds of a reversible reaction rather than as heat, is one of the most promising routes to fill this gap, and it is the family to which the system studied in this thesis belongs.

1.1.3) Solar cogeneration and district energy systems

A third relevant domain is that of cogeneration and district energy. Heating and cooling account for about half of Europe's final energy consumption, and district heating and cooling networks, well established in Northern and Eastern Europe, are recognised by EU energy-efficiency policy as a key instrument for decarbonising this demand. Cogeneration (combined heat and power) and trigeneration (combined cooling, heat and power) raise the overall efficiency of energy use by delivering two or three useful outputs, electricity, heat and cooling, from a single energy input, instead of rejecting the low-grade heat that a power-only plant discards.

The coupling of these systems with solar energy is an active field: solar district heating is expanding, particularly in Nordic countries, and increasingly relies on seasonal thermal storage to match a summer-dominated supply with a winter-dominated demand. Solar-driven trigeneration, which would supply a district with all three energy vectors from a renewable source, is comparatively unexplored, chiefly because it requires a high-temperature, dispatchable solar heat source, exactly what the combination of CSP and thermochemical storage can provide.

1.2) The opportunity: a solar trigeneration plant with calcium-based storage

The three domains outlined above converge on a clear opportunity. Solar energy is abundant and increasingly cheap, but its variability demands storage; CSP can supply dispatchable high-temperature heat, but the molten-salt storage it usually relies on is limited to a few hours and cannot bridge multi-day or seasonal deficits; district energy systems could decarbonise a large share of heating and cooling demand, but lack a renewable, high-temperature, long-duration heat source to draw upon. A technology able to store solar heat for days or weeks, without degradation and at low cost, would connect these threads.

Thermochemical storage based on the calcium hydroxide cycle offers precisely these features. By storing energy in the reversible reaction between calcium oxide and water, it decouples energy from temperature and allows the storage medium to be kept at ambient conditions indefinitely, using an abundant, cheap and non-toxic material. Integrating this storage with a CSP plant, and using the recovered heat to drive a trigeneration block, yields a system that can supply electricity, heating, domestic hot water and cooling to a residential district almost entirely from solar energy, throughout the year. It is this opportunity, a CSP plant coupled to $CaO/Ca(OH)_2$ thermochemical storage and a trigeneration block serving a district, that the present thesis sets out to design and assess. The following sections describe the storage technology in detail and state the objectives and methodology of the work.

1.3) Calcium oxide based energy storage

The core of this thermochemical energy storage system is the reversible chemical reaction between calcium oxide (CaO) and water (H2O). The $CaO/Ca(OH)_2$ cycle for energy storage is divided into two distinct operational phases: the charging phase, based on the dehydration of calcium hydroxide, and the discharging phase, which takes place thanks to the hydration of calcium oxide.
When the power production of the renewable energy plant exceeds the power demand of the user, it is possible to store energy thanks to the dehydration of the calcium hydroxide:

$$Ca(OH)_2 + \text{heat} \rightarrow CaO + H_2O \quad \text{(charging, dehydration)}$$

The opposite situation is during no sufficient power production by a renewable energy plant, so the energy storage must provide power to the user, and so the process of discharging takes place; it is based on the calcium oxide hydration:

$$CaO + H_2O \rightarrow Ca(OH)_2 + \text{heat} \quad \text{(discharging, hydration)}$$

A fundamental distinction between the proposed system and conventional thermal energy storage (TES) lies in the energy carrier. While sensible or latent heat systems rely on maintaining a temperature gradient relative to the environment, which leads to thermal dissipation over time, the thermochemical approach preserves energy within the chemical potential of molecular bonds, so the material can be stored at ambient temperature.
This characteristic introduces three fundamental advantages for the plant's architecture:

- Indefinite Storage Duration: Once the dehydration process is complete, the resulting products (solid CaO and H2O) are chemically stable. They can be stored in atmospheric silos at ambient temperature. This reduces the cost of storage silos eliminating the necessity for expensive high-vacuum insulation or continuous reheating, allowing the system to extend the period of storage to longer duration, not only on a daily but also on a seasonal scale, eliminating the degradation of the stored power density.
- high volumetric energy density: Compared to water-based or molten salt storage, the CaO/Ca(OH)2 thermochemical energy storage system has a higher energy density (approx. 400 kWh/m3), allowing a more compact plant footprint, facilitating the integration of that type of plant into urban or industrial district heating networks.
- Cost Reduction in Infrastructure: From an engineering standpoint, the ability to store materials at ambient temperature significantly reduces the capital expenditure (CAPEX). The silos do not require multi-layer insulation systems

The operational temperature range of the CaO/Ca(OH)2 cycle is one of its most advantageous features. Unlike other thermochemical cycles that require high temperatures (in the order of 800-1000°C), this system operates within the medium-temperature range, between 450°C and 600°C.
From an engineering perspective, this "thermal window" offers several critical benefits:

- Material Compatibility: At these temperatures, the use of standard industrial alloys (such as stainless steels) is feasible, avoiding the need for expensive superalloys or ceramic linings required by high-temperature cycles.
- High-Quality Heat Dispatch: The heat released at approximately 500°C is of sufficient quality to drive a Rankine Cycle with high efficiency or to be integrated into existing industrial steam networks. This makes the system far more versatile than low-temperature storage (like domestic water tanks), which can only provide space heating.
- Thermal Management: Operating at 500-600°C allows for a favourable compromise between reaction kinetics (which are faster at higher temperatures) and the thermodynamic equilibrium, ensuring a high conversion rate in both the charging and discharging phases.

In the broader context of the energy transition, the sustainability of the storage medium itself is a decisive factor. The Calcium Oxide storage technology stands out for its exceptional environmental profile, particularly when compared to electrochemical batteries (lithium-ion) or other thermochemical systems based on heavy metals.

- Abundance and Low Cost: the storage medium is based on calcium, one of the most abundant elements in the Earth's crust. Calcium oxide and calcium hydroxide are widely distributed, abundant, inexpensive and sustainable materials, derived from raw sources that are available worldwide. This abundance minimises both the geopolitical risks and the carbon footprint associated with the supply chain, and it is one of the decisive advantages of the $CaO/Ca(OH)_2$ system over storage technologies that rely on scarce or critical materials.
- Non-Toxicity and Safety: Both Calcium Oxide and Calcium Hydroxide are non-toxic and non-flammable materials. Unlike lithium batteries, which pose risks of thermal runaway and fire, or molten salts, which can be corrosive and hazardous if leaked, CaO is chemically stable and safe to handle.
- Ease of Decommissioning: At the end of the plant's operational life, the materials do not require complex waste treatment. They can be safely reused in other industrial fields, embodying the principles of a Circular Economy. This lack of toxicity is a key enabler for the deployment of such plants in proximity to urban areas for district heating applications.

1.3.1) Challenges of the technology

Alongside these advantages, the $CaO/Ca(OH)_2$ system presents challenges that are the object of ongoing research and that must be acknowledged in a realistic assessment.

- The most significant is the cyclic degradation of the material: repeated hydration–dehydration cycles progressively reduce the reactivity and the effective energy density of the solids, through sintering and loss of porosity, so that a fraction of the inventory must be periodically replaced, an effect accounted in the operating costs of Chapter 6.
- Transport of large quantities of powder between reactors and silos requires reliable conveying and heat-recovery systems, and the gas-solid reactors must sustain good heat and mass transfer while avoiding agglomeration of the particles.
- The technology has a low commercial maturity: unlike molten-salt storage, the $CaO/Ca(OH)_2$ cycle has so far been demonstrated mainly at laboratory and pilot scale, which introduces uncertainty in the cost estimates of the reactors and in the scale-up to the sizes considered in this work. These aspects do not undermine the potential of the technology, but they define the directions in which it must still progress to reach full industrial deployment.

1.4) Renewable integration

The full decarbonization of the energy cycle proposed in this study is achieved through the direct integration of the thermochemical storage plant with a Concentrated Solar Power (CSP) system. Unlike traditional photovoltaic (PV) systems, which convert solar radiation into electricity, CSP technology utilizes mirrors or lenses to concentrate a large area of sunlight onto a receiver. This thermal approach is inherently compatible with the $CaO/Ca(OH)_2$ cycle, as it provides the required high-temperature heat directly to the charging reactor.

The choice of CSP as the primary energy source is dictated by the thermodynamic requirements of the calcium hydroxide dehydration reaction. As previously analysed, the charging phase requires temperatures consistently exceeding 550°C to achieve efficient kinetics and high conversion rates.

Among the various renewable configurations, CSP, specifically Central Receiver Systems (Solar Towers), can provide steady thermal power at temperatures reaching 600°C and beyond. This temperature level ensures that the Ca(OH)2 can be fully decomposed into CaO, effectively transforming the concentrated solar flux into stable chemical potential. By utilizing a solar tower configuration, the plant can achieve the necessary concentration ratios to maintain the reactor's operational setpoint, even during periods of variable solar DNI (Direct Normal Irradiance).

The integration of a $CaO/Ca(OH)_2$ storage system with a CSP plant addresses the "dispatchability" problem of solar energy. While a standard CSP plant might use molten salts for short-term storage (limited to 10-15 hours), the coupling with the calcium hydroxide cycle extends this capability to long-term and seasonal scales.

In this configuration, the CSP field acts as the "prime mover" during daylight hours, driving the endothermic reaction and producing the CaO "fuel". This "fuel" is then stored at ambient temperature, ready to be used during the night or period of lower solar irradiance due to bad weather condition. This synergy transforms the CSP plant from a simple daytime power generator into a fully dispatchable energy hub, capable of matching the user demand curve regardless of the solar cycle.

1.5) Justification of the work

The choice of the $CaO/Ca(OH)_2$ cycle as the storage technology for this plant follows directly from the comparison outlined in Section 1.2.2, and rests on three criteria: thermodynamic efficiency, economic sustainability and operational stability.
Against the molten-salt storage that represents the industrial benchmark in CSP plants, the thermochemical approach has the decisive advantage of decoupling energy from temperature: once the endothermic dehydration reaction is complete, the solid products and water can be stored at ambient temperature for indefinite periods, without the thermal dissipation that limits sensible-heat systems to a few hours of autonomy.
Against electrochemical storage, which is optimised for short-duration peak management but prohibitive for large-scale, long-duration use, the $CaO/Ca(OH)_2$ system relies on calcium oxide and calcium hydroxide, among the most abundant and inexpensive materials on Earth, free from the scarcity, flammability and toxicity concerns of lithium-based batteries. Finally, its environmental profile aligns with the paradigms of the Circular Economy: at end of life the calcium-based solids can be repurposed in related industrial sectors, such as construction or soil stabilisation. The ability to integrate the storage directly with a high-temperature solar source, avoiding the conversion losses of intermediate electricity-to-heat stages, confirms the $CaO/Ca(OH)_2$ cycle as an efficient pathway toward a large-scale, flexible and fully dispatchable thermal storage system.

1.6) Objective

The primary objective of this thesis is the design and performance analysis of a thermochemical energy storage system based on the $CaO/Ca(OH)_2$ cycle, integrated with a Concentrated Solar Power (CSP) plant.
This research aims to achieve the following specific goals:

- System Integration and Sizing: To develop a process layout capable of meeting the power, thermal and cooling demand, sizing the main components, specifically the dehydration and hydration reactors and the storage silos, based on thermodynamic mass and energy balances.
- Operational Mode Definition: To define the operational strategy of the plant, establishing a cyclic process that effectively manages the intermittent nature of solar energy by switching between the "Charging" and "Discharging" modes.
- Process Simulation and Validation: To model the power block and the main process streams in the DWSIM process simulator, closing the mass and energy

balances of the plant and verifying the consistency of the sizing across the different operating modes.
- Performance Assessment: To evaluate the system's efficiency in terms of chemical potential storage and heat release, demonstrating the technical feasibility of using calcium-based materials for long-duration, high-temperature thermal energy storage.

Through these objectives, this study seeks to provide a scalable framework for industrial-scale solar thermal storage, overcoming the current limitations of sensible heat technologies and contributing to the transition toward fully dispatchable renewable energy hubs.

1.7) Methodology

The methodology followed in this thesis moves from the theoretical characterisation of the storage reaction to the sizing of the plant, its operational modelling over the year, and finally its techno-economic assessment.

The work is organised in four phases.

- Thermodynamic characterisation: The first phase establishes the thermodynamic basis of the $CaO/Ca(OH)_2$ cycle, evaluating the reaction enthalpy and the equilibrium conditions of the dehydration and hydration reactions in order to fix the operating temperatures of the two reactors and to confirm the compatibility of the cycle with the high-temperature heat supplied by the CSP receiver.
- Process modelling in DWSIM: The power block and the main process streams are modelled in the DWSIM process simulator, using the IAPWS-IF97 steam tables for the steam Rankine cycle built around the Siemens SST-200 turbine. DWSIM is used to close the mass and energy balances of the plant in its different operating modes and to verify the consistency of the preliminary sizing.
- Plant sizing and daily energy model: Starting from the energy demand of the residential district, the main components — reactors, storage silos, turbines, trigeneration block and solar field — are sized through mass and energy balances (Chapter 3). The operation of the plant is then reproduced with a daily-resolved energy model, developed in a spreadsheet, that follows the charge and discharge of the storage across a full reference year and, on selected winter and summer design days, on an hourly basis (Chapter 4). This model is the main tool of the study: it quantifies the seasonal behaviour, the state of charge of the storage, the grid exchanges and the surplus management for each configuration.
- Configuration analysis and techno-economic assessment: On the basis of the daily model, the alternative plant configurations are compared (Chapter 5): the single- versus dual-turbine power block, and the two storage-and-coverage strategies (Scenario A and Scenario B). Finally, the techno-economic analysis (Chapter 6) estimates the capital and operating costs of each configuration and evaluates their profitability through a discounted cash-flow analysis, deriving the net present

value, the discounted payback time and the levelised cost of energy (LCOE), and testing the robustness of the results against the main cost and price uncertainties through a set of economic scenarios.

2) REFERENCE TECHNOLOGIES

The plant studied in this thesis is conceived for a specific application: the supply of electricity, heating, domestic hot water and cooling to a residential district of about 13,000 dwellings located near Seville, in southern Spain. This choice of location and scale sets the requirements around which the whole plant is designed. The region combines a high direct normal irradiance throughout the year, which makes it well suited to a central-receiver solar field, with a Mediterranean climate that imposes a marked seasonal asymmetry on the demand: winter is dominated by space heating and domestic hot water, summer by the cooling load, while in the intermediate seasons electricity becomes the leading service. Serving this shifting, multi-vector demand from a single solar source, whose availability follows its own independent cycle, is the central challenge that the plant is designed to address, and it is what motivates the coupling of concentrated solar power with long-duration thermochemical storage. The size of the district fixes the magnitude of the energy flows and, with them, the sizing of every component. On this basis, the present chapter describes the reference technologies that make up the plant and the way they are integrated; their quantitative sizing, together with the detailed definition of the demand profiles and the design assumptions, is developed in Chapter 3.

2.1) General schematic of the plant

The technical analysis of this research is centered on the development of a highly integrated energy hub designed to provide a continuous and reliable supply of multiple energy vectors, power, heat and cold to the user. The complexity of the system arises from the need to synchronize a fluctuating, on a daily and seasonal basis, renewable source with a constant and diversified energy demand by the end user. To achieve this, the plant architecture is organized into three fundamental macro-blocks that operate in synergy: the Concentrated Solar Power (CSP) field, the $CaO/Ca(OH)_2$ thermochemical energy storage system, and the multi-vector Trigeneration Plant. The integration of these three blocks represents a holistic approach to energy management, where the production, storage, and final delivery of energy are optimized to ensure maximum global efficiency and full dispatchability, thanks to the storage that can cover the mismatch between the supply curve and the demand one, on a period of up to a few days, to cover period of no production by the CSP due to weather conditions lasting longer than a single night.

The first block, the Concentrated Solar Power (CSP) field, serves as the primary thermal engine of the entire infrastructure. Its role is to collect and concentrate direct normal irradiance (DNI) to generate high-temperature thermal energy. This solar heat represents the energy source of the system, but its inherent intermittency, caused by the day-night cycle and weather variability, necessitates a robust interface capable of balancing energy supply and demand. In this architecture, the CSP field does not directly drive the power cycle in a rigid configuration; instead, it acts as a flexible thermal source that can simultaneously power the production plant and the storage system, depending

on the instantaneous solar availability and the operational strategy adopted. The thermal power feeds the trigeneration power plant and the excess is stored in the chemical storage.
The second core component is the $CaO/Ca(OH)_2$ energy storage system, which acts as the "thermal buffer" or chemical battery of the hub. This block is what distinguishes the proposed plant from conventional solar installations. By utilizing the reversible chemical reaction between calcium oxide (CaO) and water vapor, this section can store vast amounts of solar energy in the form of chemical potential. During periods of high solar irradiance, the excess heat from the CSP is diverted to the storage block to "charge" the system through an endothermic dehydration process. Conversely, during the night or overcast periods, the system is "discharged" through an exothermic hydration reaction, releasing high-grade heat. This block is essential for decoupling the primary energy collection from the final energy delivery, allowing the plant to remain operational even in the absence of direct sunlight.
The third and final block is the Trigeneration Plant, which represents the direct interface with the end-user. This section is designed to transform the thermal energy, originating either directly from the CSP field or recovered from recovered from the thermochemical storage, into three distinct energy services: electricity, heating, and cooling. The goal of the trigeneration block is to maximize the second-law efficiency of the plant by utilizing waste heat recovery for thermal purposes (heating) and absorption chilling cycles (cooling), alongside the primary electrical power generation. This multi-vector output is specifically tailored to meet the complex and fluctuating needs of the user, ensuring that every unit of thermal energy generated is exploited to its fullest potential. The specific configuration of the trigeneration has to be chosen taking into account the type of user demand.
The synergy between these three blocks creates a resilient and flexible energy ecosystem. While the CSP field provides the raw energy input, the thermochemical storage ensures the system's stability and autonomy, and the Trigeneration plant provides the final, high-value services to the user. This integrated approach allows for a "load-following" operational logic, where the plant can adapt its output based on the specific demands of the user rather than being constrained by the availability of the solar source.

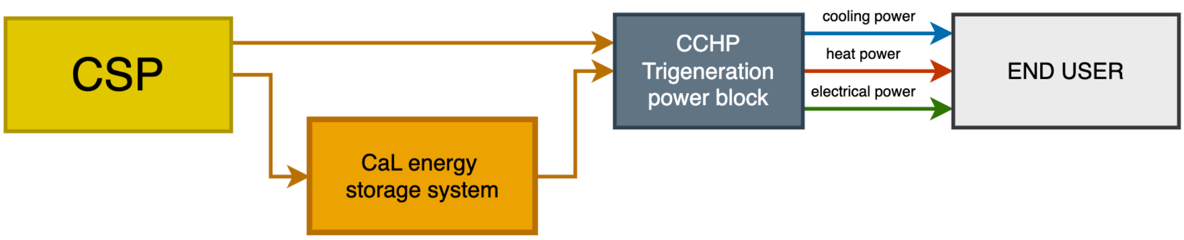

Figure 2.1 General schematic of the integrated plant, showing the three macro-blocks

2.2) $CaO/Ca(OH)_2$ thermochemical storage

The operational heart of the energy storage section is based on the reversible chemical reaction between calcium oxide (CaO) and water vapor (H2O), a process known as the $CaO/Ca(OH)_2$ hydration/dehydration cycle. This thermochemical route is particularly advantageous for high-temperature energy storage due to the high energy density of the materials involved and the complete reversibility of the reaction. The chemical equilibrium governing the entire process can be expressed as follows:

$$Ca(OH)_2 \leftrightarrow \mathrm{CaO} + H_2O \quad \Delta\mathrm{H} = \pm 104.4\ \mathrm{kJ/mol}$$

The cycle is divided into two distinct functional phases: the charging phase (endothermic) and the discharging phase (exothermic). During the charging phase, the system behaves as an energy sink. Thermal energy collected by the CSP field is transferred to the dehydration reactor, where the calcium hydroxide (Ca(OH)2) is heated above its decomposition temperature (typically between 450°C and 550°C, depending on the partial pressure of the steam). At this stage, the chemical bonds are broken, absorbing the solar heat and converting it into chemical potential. The products of this reaction are solid calcium oxide (CaO) and water vapor. The steam is subsequently separated and condensed, while the "charged" CaO is conveyed to atmospheric silos. This allows the energy to be stored in a stable, solid form at ambient temperature, effectively eliminating the thermal standby losses that characterize sensible heat storage systems.
Conversely, the discharging phase is initiated when there is a demand for energy from the user or when the solar source is unavailable. During this phase, the stored calcium oxide is transported from the silos to the hydration reactor, where it is put back into contact with water vapor. This recombination triggers a highly exothermic reaction, as the CaO recombine with vapour to return to its original state as calcium hydroxide (Ca(OH)2). The chemical potential stored during the day is released in the form of high-grade heat. The temperature of this heat release is governed by the thermodynamic equilibrium of the system; by controlling the pressure and the steam flow rate, the reactor can provide a stable thermal output at temperatures suitable for driving the steam turbines or heat exchangers of the trigeneration plant.

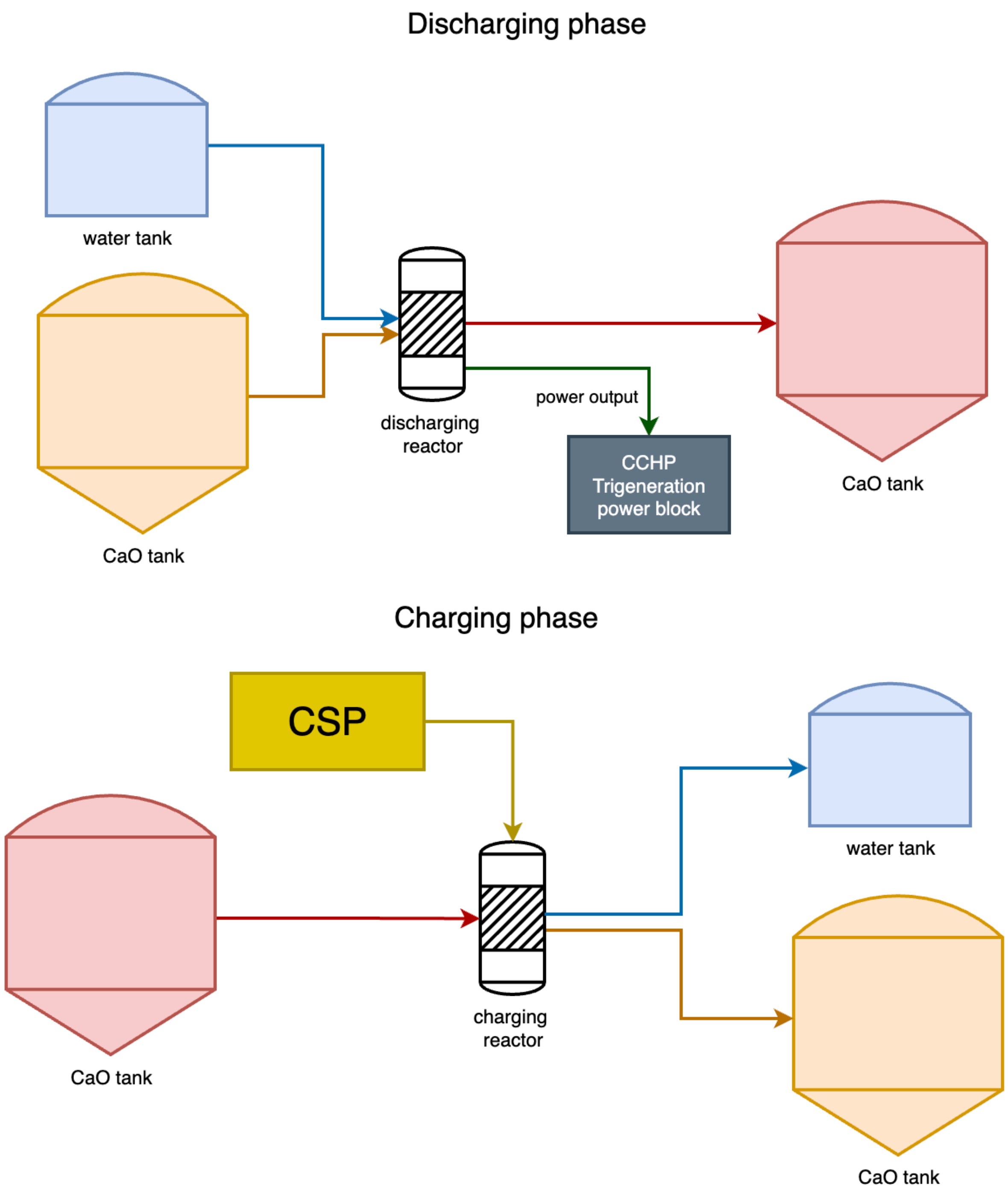

Figure 2.2 The two phases of the CaO/Ca(OH)$_2$ cycle: endothermic dehydration and exothermic hydration

To fully understand the plant's operational autonomy, it is essential to analyze the mechanical interaction between the storage tanks and the reaction units, to form the complete calcium-based storage system. The system is designed as a closed-loop solid cycle, where the total inventory of calcium-based material remains constant within the plant, moving between different chemical states and storage temperatures. The two main silos, one for the "charged" Calcium Oxide (CaO) and one for the "discharged" Calcium Hydroxide (Ca(OH)2), act as the primary mass reservoirs, then ther's another one smaller to store ne water needed in the reaction. The total mass of the calcium based material will be evaluated on the bases of the necessary storage time needed and the user power demand by the end user, and to guarantee effective decoupling of the chemical kinetics of the reactors from the daily solar cycle.

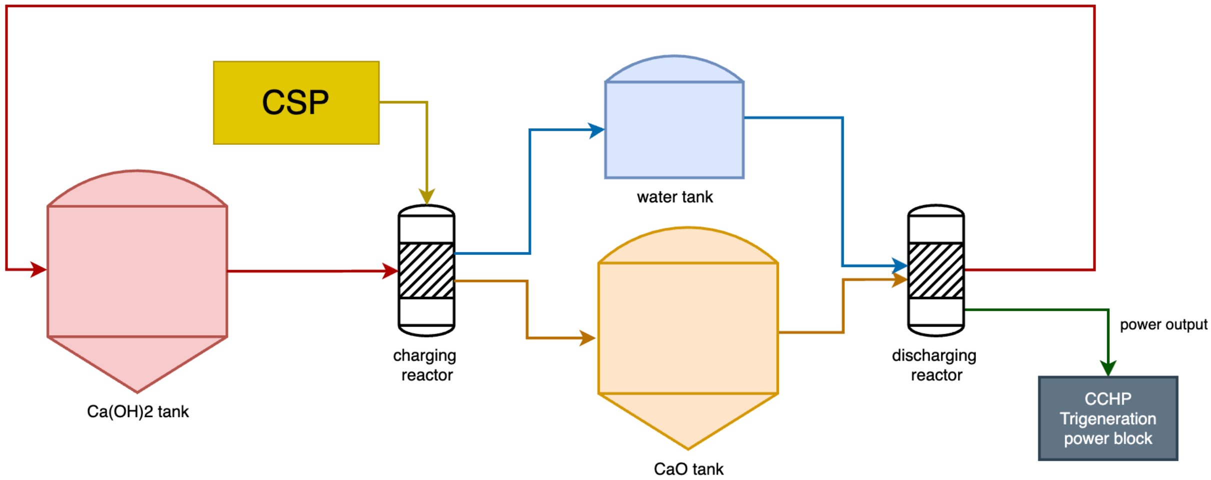

Figure 2.3 Layout of the storage section: the silos holding and their connection to the reactors in a closed-loop cycle

2.3) Heat exchanger system

A critical advancement in the plant's architecture is the integration of high-temperature heat exchangers designed to optimize the thermal management of the solid streams. While the basic configuration establishes the mass balance between silos and reactors, the overall energy efficiency of the $CaO/Ca(OH)_2$ cycle is heavily dependent on the ability to recover sensible heat. In both the charging and discharging phases, there is a significant temperature gradient between the material stored in the atmospheric silos (at ambient temperature) and the operational setpoints of the reactors (ranging from 450°C to 600°C).

In the Charging Phase, the calcium hydroxide (Ca(OH)2) entering the dehydration reactor must be pre-heated to minimize the direct thermal load on the CSP receiver. By implementing a solid-solid heat exchanger, the "cold" stream of Ca(OH)2 is pre-heated by the "hot" stream of calcium oxide (CaO) and the water one exiting the reactor. This internal heat exchange not only protects the reactor from thermal shock but also significantly reduces the solar field area required to drive the endothermic reaction, as a substantial portion of the sensible heat is kept within the loop.

Similarly, during the Discharging Phase, a symmetrical recovery logic is applied. The "cold" CaO and water leaving the storage silo are pre-heated by the "hot" Ca(OH)2 that has just completed the exothermic hydration process. This recovery is vital for the trigeneration plant's performance: by ensuring that the solids enter the hydration reactor already at an elevated temperature, the reaction kinetics are accelerated, and the high-grade heat released by the chemical reaction can be fully dedicated to the user demand rather than being partially consumed to heat the incoming mass.

The inclusion of these heat exchangers transforms the plant from a simple storage unit into a highly integrated thermal network. This configuration ensures that the sensible heat is effectively "recycled" within the process. This minimization of thermal waste is what allows this thermochemical technology to compete with traditional storage systems, providing a high-temperature output with a superior global energy performance.

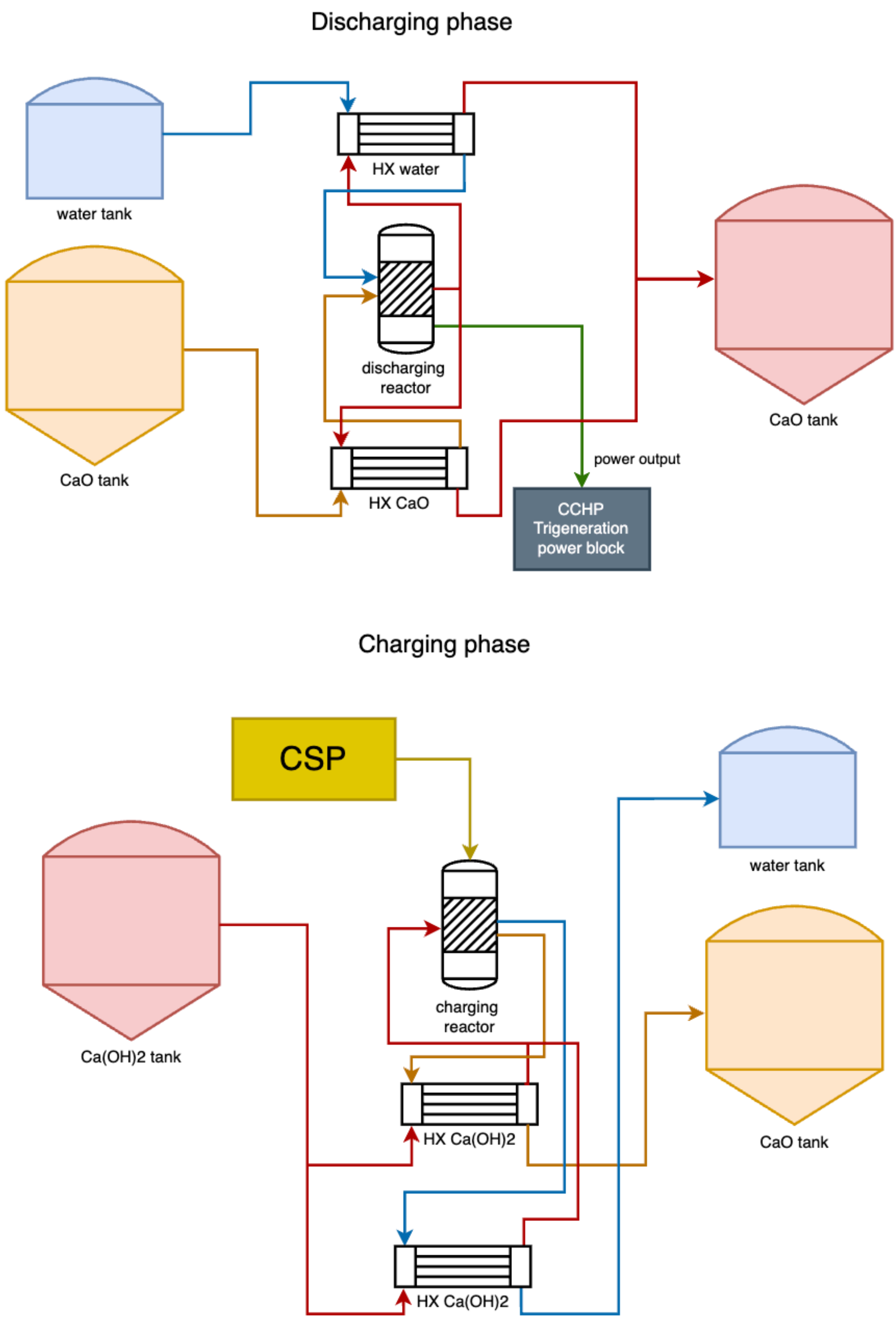

Figure 2.4 Heat-exchanger network of the storage section

2.4) Direct connection storage-user

A fundamental design choice explored in this study is the implementation of a multi-stage thermal recovery strategy, designed to cascade the heat according to its quality and temperature grade. This approach recognizes that the thermal energy contained in the streams exiting the reactors, both during the endothermic charging and the exothermic discharging stages, is a high-value asset that must be managed with a strict priority logic. The primary objective is the internal pre-heating of the input flows: by redirecting a significant fraction of the exit heat to the incoming "cold" materials (the storage precursors), the system effectively reduces the external energy required to trigger the chemical reactions, thereby maximizing the intrinsic efficiency of the $CaO/Ca(OH)_2$ cycle.

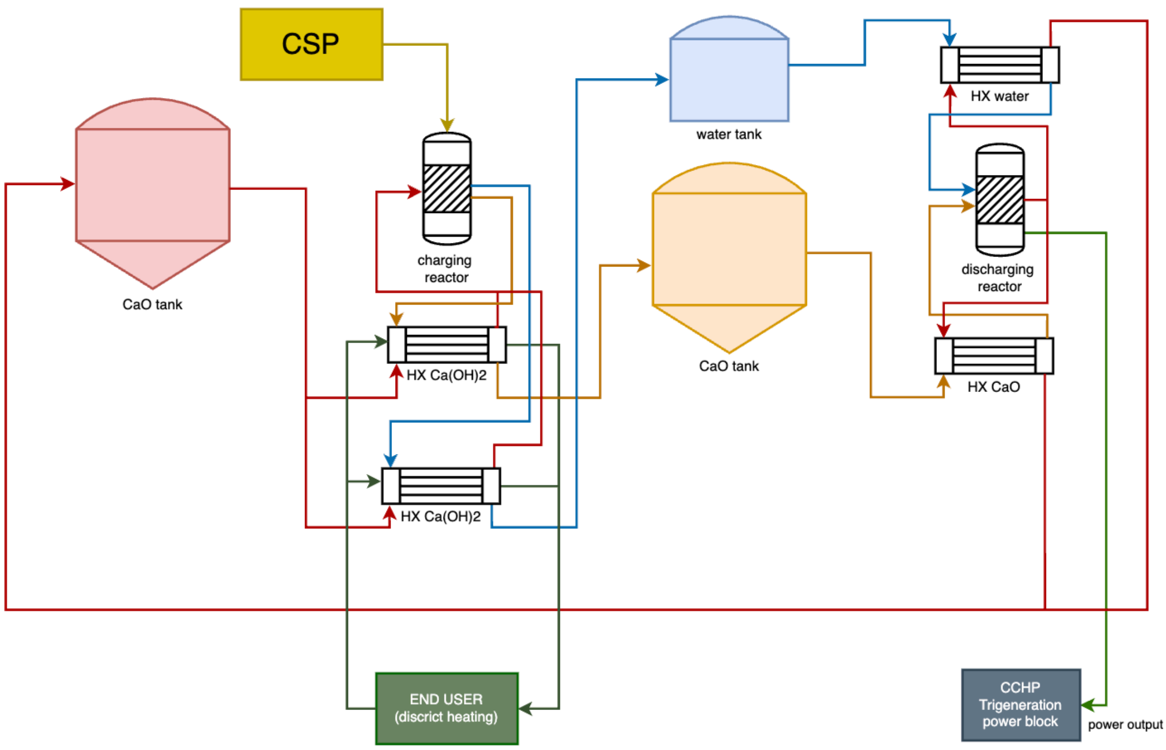

Figure 2.5 Cascade of the recovered heat

However, the analysis also considers the potential availability of a thermal surplus. In scenarios where the sensible heat of the output streams exceeds the requirements for internal pre-heating, the plant architecture is designed to avoid any energy dissipation. Instead of wasting this excess heat through atmospheric cooling, the system allows for its direct export to the end-user. This secondary recovery stage can be seamlessly integrated into district heating networks or low-to-medium temperature industrial processes. By adopting this "internal-first, external-second" recovery priority, the plant does not only function as a power storage unit but also as a high-efficiency thermal hub, ensuring that every kilowatt-hour of solar energy captured is either stored or utilized to meet a specific user demand.

2.5) Components

Having described the functional architecture of the plant and the logic governing its thermal integration, this section provides a component-level overview of the main equipment that physically realises the three macro-blocks. Each item is presented in terms of its engineering function and the technological options considered; the detailed sizing of every unit is addressed in the dedicated chapter.

Concentrated Solar Collector. The collector adopts a central receiver (solar tower) configuration. A field of dual-axis tracking heliostats reflects and concentrates the direct normal irradiance onto a single receiver mounted at the top of a tower. The high concentration ratio achievable with this layout allows the receiver to reach the temperature required to drive the dehydration reaction, a level that distributed-collector technologies such as parabolic troughs or linear Fresnel cannot reliably sustain. The receiver, of external or cavity type, transfers the concentrated flux to the heat-transfer medium that feeds the charging reactor. Being the only component directly exposed to solar variability, the collector is also the element that imposes the intermittent boundary condition the rest of the plant is designed to absorb.

Tank. The storage inventory is held in three separate atmospheric vessels: one silo for the charged calcium oxide, one for the discharged calcium hydroxide, and a smaller liquid tank for the process water released and reabsorbed during the cycle. The solid silos are vertical cylindrical vessels with a conical lower section to promote gravity-assisted discharge, equipped with the aeration and fluidization aids typical of fine-powder handling. Since the solids are stored cold and chemically stable, the vessels are conventional steel constructions, which directly conditions both their cost and their structural design. The water tank closes the mass balance of the loop, buffering the steam that is condensed during charging and supplied back during discharging.

Heat exchanger. Two families of heat exchangers coexist in the plant. On the solids side, high-temperature solid–solid units, of moving-bed or screw type suited to granular media, recover the sensible heat of the streams leaving the reactors, while gas–solid units handle the steam released and supplied by the reactions. On the power side, conventional exchangers perform the standard duties of the trigeneration block: the steam generator that raises steam from the heat of hydration, the condenser, and the water-to-water exchangers that transfer heat to the district network.

Valve. Valves provide the control degrees of freedom that make the plant dispatchable. On the steam side, the extraction valve on the turbine modulates the bleed fraction diverted to thermal uses, while additional throttling and isolation valves route the flow between charging and discharging operation. On the solids side, rotary valves and slide gates regulate the mass flow of powder discharged from the silos toward the reactors. Pressure-relief and safety valves complete the set, protecting the high-temperature sections of the circuit.

Pipe. The connecting network comprises three distinct transport systems. High-temperature steam lines, fabricated in suitable alloy and thermally insulated, carry the working vapour between reactors, exchangers and the power block. The granular solids are not piped in the conventional sense but moved through mechanical conveyors of screw or bucket type, or through pneumatic conveying lines sized for the powder flow rate. A simpler water-side circuit links the liquid tank with the points of condensation and injection. Material selection and insulation of the hot lines are dictated by the operating temperature window of the storage section.

Reactor. The reactors are the gas–solid contactors where the storage reaction is carried out. Charging takes place in the dehydration reactor, where heat from the solar receiver decomposes the calcium hydroxide; discharging takes place in the hydration reactor, where steam is recombined with the calcium oxide to release high-grade heat. Both duties can be realised as fluidized-, moving- or fixed-bed units, the choice being a trade-off between conversion, pressure drop and ease of solids handling. In the process model they are represented as equilibrium reactors, an assumption that captures the conversion attainable at the prevailing temperature and steam partial pressure while keeping the simulation tractable.

Trigeneration. The trigeneration block groups the equipment that converts the stored thermal energy into the three energy services delivered to the district. A steam generator raises steam from the heat released by the hydration reactor; this steam expands in a steam turbine of 10 MWe nominal capacity, fitted with a variable extraction stage that allows part of the flow to be bled for thermal duties. The remaining flow is condensed, while the alternator coupled to the turbine delivers the electrical output. For the cooling service, a double-effect absorption chiller is driven by extracted steam during the summer, while dedicated heat exchangers feed the district heating and domestic-hot-water networks. The way these units are operated across the seasons is detailed in the sizing section.

2.6) Operation modes

The plant is operated according to a load-following logic in which the instantaneous role of the storage section is dictated by the balance between the thermal power made available by the solar field and the energy demanded by the district. Three operating regimes can be distinguished: daylight operation, dark-hour operation, and the transient phases of start-up and shut-down.

Sun hours. During daylight the solar receiver delivers thermal power to the plant, and the operating point depends on the instantaneous match between this power and the user demand. When the collected solar power exceeds the demand, the surplus is diverted to the dehydration reactor and the storage section operates in charging mode: while the trigeneration block is supplied with the share of solar heat needed to cover the current load, the excess decomposes the calcium hydroxide and accumulates chemical potential in the silos. The opposite situation arises whenever the available solar power falls short of the demand, as happens at the beginning and end of the day or during cloud transients: the solar input alone cannot sustain the load, so the hydration reactor is activated and the storage operates in discharging mode, supplementing the direct solar contribution. Daylight operation is therefore not a purely charging window, but a regime in which charging and discharging can alternate according to the real-time energy balance, with the storage absorbing every mismatch in either direction.

Dark hours. In the absence of solar irradiance the district demand is met entirely by discharging the storage: calcium oxide is conveyed from the silo to the hydration reactor, where the exothermic recombination with steam releases the high-grade heat that drives the trigeneration block throughout the night. Because the thermal response of a solid-gas reactor is governed by reaction kinetics and by the inertia of the solid streams, its output cannot follow the sharp variations of the user demand instantaneously. To decouple the reactor from these fast fluctuations, a steam (Ruths-type) accumulator is integrated on the steam side, between the steam generator fed by the hydration heat and the turbine. Storing energy as pressurised saturated water, the accumulator releases additional steam as soon as its pressure is lowered, thereby responding to load transients far faster than the reactor itself. This allows the hydration reactor to be operated at a steadier rate, well suited to its kinetics, while the accumulator absorbs the short-term mismatch with the variable district demand. Its function is one of rapid-response buffering over the scale of minutes to a few hours; the long-duration energy reserve remains entirely entrusted to the thermochemical storage.

Start-up and shut-down. The transient phases require dedicated attention because the reactors and the solid inventory possess a significant thermal inertia, so that a finite time is needed to bring the units to their operating setpoint. During start-up, before the hydration reactor reaches a stable high-grade output suitable for the power block, the sensible heat carried by the hot streams leaving the reactor can be routed directly to the lower-grade user services, namely district heating and domestic hot water, rather than being dissipated. The same recovery logic applies during shut-down, when the residual sensible heat retained by the solids and by the circuit is delivered to these thermal users while the plant is brought to rest. Exploiting the after-reactor heat in this way limits the energy penalty associated with the transients and ensures that the plant continues to provide a useful output even when it is not operating at its nominal regime.

2.7) Application

The architecture described in the previous sections is general in nature and could in principle serve different categories of end-user, ranging from industrial processes requiring high-temperature heat to combined supply schemes for civil settlements. Among these possibilities, this study applies the integrated plant to a residential district. The choice is motivated by the close match between the multi-vector output of the trigeneration block, which simultaneously provides electricity, heating and cooling, and the diversified energy needs of a residential community. A residential application is also the most demanding test for the storage concept: domestic demand is strongly variable on both the daily and the seasonal scale, and it is precisely under such fluctuating conditions that a long-duration storage demonstrates its value. Finally, the non-toxic and intrinsically safe nature of the calcium-based storage medium is a decisive enabler for this application, as it allows the plant to be sited in proximity to inhabited areas and to be connected to a district heating and cooling network without the safety constraints associated with other storage technologies.

The role of the integrated plant in this context is to behave as a self-contained and fully dispatchable energy hub. The district requires a continuous and reliable supply of the three energy services, whereas the solar resource is available only intermittently and is systematically out of phase with the demand, both on the daily scale, because of the day-night cycle, and on the multi-day scale, because of prolonged periods of low irradiance. The function of the storage section is to bridge this mismatch entirely, decoupling the delivery of energy to the user from the instantaneous availability of the sun and allowing the plant to follow the load of the district at all times.

The development of the case study considers two distinct operating philosophies for the storage, which represent two points along the trade-off between energy independence and capital cost: a quasi-autonomous configuration, with a large storage that reduces the recourse to the grid to a few critical winter days, and a grid-assisted configuration, with a more compact storage and a heavier reliance on the grid. These two strategies are introduced here only at the conceptual level; their quantitative definition and the detailed sizing of every component of the plant, including the user demand, the trigeneration block, the solar field and the storage, are the subject of the following chapter.

3) PLANT SIZING

Design assumptions and methodology

The plant is sized at the design point through steady-state mass and energy balances, with each component dimensioned at its nominal operating condition. The two reactors are treated as equilibrium units, so that the conversion is the one allowed by the temperature and the steam partial pressure; kinetic effects are not resolved at this stage, and their macroscopic impact is retained through the loss factors introduced where relevant.
The calculation follows a chain anchored to the power block. The turbine fixes the thermal scale of the plant; the district demand, defined consistently with the turbine, sets the heat to be supplied together with electricity; the demand integrated over the days of autonomy fixes the storage inventory; and the power required to serve the load and charge the storage sizes the solar field. The procedure is carried out in parallel for the two scenarios defined in the previous chapter, the quasi-autonomous Scenario A and the grid-assisted Scenario B, which share the same models and differ only in the prescribed autonomy and in the coverage criterion applied on the critical days. The parameters of each component are introduced in the section where that component is sized.

3.1) Power block: steam turbine selection and sizing

The sizing starts from the power block, because the turbine is the component with the least freedom: steam turbines are produced in fixed frames with a defined power range, while the other sections can be scaled continuously. The machine is therefore fixed first, and the rest of the plant is sized around it.
The nominal electrical power is set at 10 MWe, a typical value for a district-scale unit. The sizing carried out in this chapter refers to a single extraction turbine, which serves the whole demand of the district and constitutes the reference power block. The possibility of adding a second turbine, dedicated to recovering the solar surplus that would otherwise be defocused and to exporting the corresponding electricity to the grid, is introduced in Chapter 4 and analysed in Chapter 5; the values found here refer to the first turbine and hold for both layouts.
The machine chosen for the reference layout is a Siemens SST-200. It covers the 10 MWe target with margin, it offers a controlled extraction stage, and its live-steam temperature, up to about 540 °C, matches the discharge temperature of the reactor. The controlled extraction is the key feature, because it lets part of the steam be bled from the turbine to supply heat: the same machine then produces both electricity and heat, and can shift the balance between them over the year.
The thermal power that the storage must send to the turbine follows from the nominal power and the cycle efficiency:

$$Q_{turb} = \frac{P_{nom}}{\eta_t} = \frac{10}{0.36} = 27.8 \text{ MW}_{th}$$

where $P_{nom} = 10 \text{ MW}_e$ is the nominal electrical power and $\eta_t = 0.36$ is the net efficiency of the steam cycle, taken as a consolidated design value representative of steam turbines of this size. This thermal power of 27.8 MWth is tied to electricity production and is the starting quantity for all the sizing that follows.

3.2) District definition and energy demand

3.2.1) Energy demand of a single dwelling

The district is sized so that its peak electrical demand equals the nominal power of the turbine. The demand is first defined for a single dwelling of 100 m^2 and then scaled to the whole district. Four services are considered, each with a specific annual demand per square metre: space heating 30, domestic hot water (DHW) 15, cooling 17 and electricity 30 kWh/(m^2·yr). The first three form the thermal demand of 62 kWh/(m^2·yr), which with electricity gives a total of 92 kWh/(m^2·yr). The cooling figure is the heat supplied to the absorption chiller, so it already belongs to the thermal demand. Heating and cooling are seasonal, lasting about four months per year (2928 h), while DHW and electricity last all year (8760 h).
For each service, the mean power of one dwelling is the annual energy divided by the hours over which the service is active, and the peak power is the mean power multiplied by a peak factor that expresses the ratio between the maximum and the mean load:

$$\bar{p} = \frac{E_{year}}{h} \qquad \hat{p} = \bar{p} \cdot f$$

The peak factors differ among services according to their nature: DHW and electricity, concentrated in a few hours, have the highest factors, while space heating, a more continuous load, has the lowest. The resulting values for a single dwelling are given below.

Service	Annual energy [kWh/yr]	Hours [h]	Mean power [kW]	Peak factor	Peak power [kW]
Space heating	3000	2928	1.025	1.3	1.332
DHW	1500	8760	0.171	2.5	0.428
Cooling (heat to chiller)	1700	2928	0.581	1.4	0.813
Electricity	3000	8760	0.342	2.0	0.685

3.2.2) Size of the district and peak demand

The number of dwellings comes from the sizing rule, namely that the peak electrical demand of the district must equal the nominal power of the turbine:

$$\boldsymbol{N = \frac{P_{nom}}{\hat{p}_{el}} = \frac{10000}{0.685} \approx 14600}$$

A rounded value of 13 000 dwellings is adopted, which leaves a margin between the resulting peak electrical demand, about 8.9 MW, and the 10 MW installed. The district therefore counts 13 000 dwellings, about 32 500 inhabitants and a floor area of 1 300 000 m^2.

The thermal power sent to the turbine is fixed at 27.8 MW. In addition, the district needs heat, which varies with the season. Scaling the per-dwelling peak powers to the whole district, the peak thermal demand beyond electricity is about 22.9 MW in winter (heating and DHW), 16.1 MW in summer (DHW and cooling) and 5.6 MW in mid-season (DHW only). The largest discharge from the storage occurs in winter, when the heat demand and the electrical demand coincide:

$$\boldsymbol{\dot{Q}_{max} = Q_{turb} + \hat{Q}_{winter} = 27.8 + 22.9 = 50.7} \text{ MW}$$

This is the maximum power that the storage and the hydration reactor must be able to deliver, and it sizes the discharge capacity of the thermochemical section.

3.2.3) Daily energy from the storage

While the peak fixes the power, the size of the storage depends on the energy used in one day, computed for the winter design day from the mean demands of 4.45 MW electrical and 15.55 MW thermal. Between the storage and the user there are losses, described by four efficiencies: $\eta_t = 0.36$ (turbine), $\eta_{sg} = 0.98$ (storage-to-steam-generator exchanger), $\eta_{dh} = 0.97$ (storage-to-district-heating exchanger) and $\eta_{net} = 0.90$ (district-heating network). Because of these losses the power drawn from the storage exceeds the demand, and splits into an electrical and a thermal part:

$$Q_{el,st} = \frac{\bar{P}_{el}}{\eta_t \cdot \eta_{sg}} = \frac{4.45}{0.36 \cdot 0.98} = 12.6 \text{ MW}$$

$$Q_{heat,st} = \frac{\bar{Q}_{heat}}{\eta_{net} \cdot \eta_{dh}} = \frac{15.55}{0.90 \cdot 0.97} = 17.8 \text{ MW}$$

Two ways of supplying the heat are compared. In the separate feed, electricity and heat are drawn from the storage independently, and the daily energy is the sum of the two contributions over 24 hours:

$$E_{sep} = \left(Q_{el,st} + Q_{heat,st}\right) \cdot 24 = 30.4 \cdot 24 = 730.2 \text{ MWh/day}$$

In the extraction feed, the heat is instead supplied by extracting steam from the turbine. The extraction lowers the electrical output by $\beta = 0.25$ MWe per MWth extracted, so more steam must pass through the cycle:

$$q_{cycle} = \frac{\bar{P}_{el} + \beta \cdot Q_{heat,st}}{\eta_t} = \frac{4.45 + 0.25 \cdot 17.8}{0.36} = 24.7 \text{ MW}$$

$$q_{storage} = \frac{q_{cycle}}{\eta_{sg}} = 25.2 \text{ MW} \quad \Rightarrow \quad E_{extr} = 25.2 \cdot 24 = 605.7 \text{ MWh/day}$$

The extraction feed draws less energy from the storage, 606 against 730 MWh/day, by exploiting steam that would otherwise be condensed; it is therefore the configuration adopted, and the resulting winter design-day energy of 605.7 MWh/day is the baseline for the storage sizing in Section 3.6.

3.3) Trigeneration sizing

The trigeneration block converts the thermal power delivered by the storage into the three services required by the district. The electrical side is already sized in Section 3.2: the 10 MWe turbine, fed by 27.8 MWth, produces the electricity and, through its controlled extraction, the steam for the thermal services. This section sizes the two thermal interfaces of the block, while the seasonal sharing of the steam among the services is treated in the operational analysis of Chapter 4.

The heat for space heating and domestic hot water is delivered to the district through dedicated exchangers fed by extracted steam, sized on the winter peak when the two demands coincide:

$$\hat{Q}_{heat} = N \cdot (\hat{p}_{heat} + \hat{p}_{dhw}) \approx 22.9 \text{ MW}$$

so the district-heating interface is sized for about 23 MW. In summer this duty drops to the DHW demand alone, and the spare extraction is redirected to cooling.

Cooling is produced by a double-effect absorption chiller driven by extracted steam, so that the service draws on the stored heat rather than on the electrical output. The cooling demand is expressed in the balance as the heat supplied to the chiller, 17 kWh/(m²·yr); the cooling effect delivered to the users follows from the coefficient of performance, taken as COP = 1.3 for a double-effect machine:

$$q_{cool} = q_{heat,chiller} \cdot COP = 17 \cdot 1.3 \approx 22 \text{ kWh/(m}^2\text{·yr)}$$

The chiller is sized on the summer peak. Scaling the per-dwelling cooling load to the district gives the peak heat to the chiller, and the cooling capacity follows from the COP:

$$\hat{Q}_{heat,chiller} = N \cdot \hat{p}_{cool} = 13000 \cdot 0.813 \approx 10.6 \text{ MW} \qquad \hat{Q}_{cool} = \hat{Q}_{heat,chiller} \cdot COP \approx 13.7 \text{ MW}$$

The chiller is therefore sized for about 13.7 MW of cooling, driven by roughly 10.6 MW of extracted heat at the summer peak. Driving it with steam rather than electricity keeps the cooling inside the thermal economy of the plant and uses steam that in summer would otherwise be only partly exploited.

3.4) Process layout and heat integration

This section fixes the process layout that connects the reactors, the storage vessels and the trigeneration block, and the heat-integration scheme that links them. The quantitative stream data follow from the process simulation; here the streams and the recovery logic are defined.

The process is a closed solid loop. During charging, calcium hydroxide is drawn from its silo, pre-heated and fed to the dehydration reactor, where the solar heat splits it into calcium oxide and steam; the oxide goes to its silo and the steam is condensed into the water tank. During discharging the path is reversed: calcium oxide and water enter the hydration reactor, which releases the high-grade heat for the power block, and the hydroxide returns to its silo. Each mode thus involves a hot stream leaving the reactor and a cold stream entering it, both crossing the wide interval between the ambient-temperature silos and the 450–600 °C reactor setpoint. For the integration analysis each stream is described by a supply temperature, a target temperature and a heat-capacity flow rate, so that its heat load is $\dot{Q} = \dot{m}\, c_p\, (T_s - T_t)$.

The integration follows the priority logic of Chapter 2: internal recovery first, external use second. The sensible heat of the streams leaving the reactor first pre-heats the streams entering it, through the solid–solid and gas–solid exchangers, minimising the external heat needed by the reactions; only the surplus is exported to the district as a lower-grade contribution. How much heat is recovered depends on the minimum approach temperature ΔT_min allowed in the exchangers, which sets the fraction of the sensible heat that can be recycled within the loop. This fraction is expressed through the reactor thermal efficiency η_th used in the storage sizing.

3.5) Thermochemical storage sizing

The storage gives the plant its dispatchability, and its sizing determines how much calcium-based material must be installed, and in how many vessels, to supply the district for the required time without sun. The procedure moves from the reaction to the energy to be stored, then to the masses, the volumes and the geometry of the silos, and finally to the losses of the real process.

3.5.1) Reaction and specific energy

The storage relies on the reversible reaction between calcium oxide and water vapour:

$$\mathrm{CaO} + \mathrm{H_2O(g)} \leftrightarrow \mathrm{Ca(OH)_2} \qquad \Delta H_r = 104.4\ \mathrm{kJ/mol}$$

Charging is the endothermic dehydration of the hydroxide, driven by the solar heat at 450–600 °C; discharging is the exothermic hydration of the oxide, which returns the stored energy as high-grade heat. Because the energy is held in chemical bonds and the charged oxide is stable at ambient temperature, the storage has negligible standing losses, and the losses of the system are concentrated in the reactors. For the sizing the energy is referred to the mass of CaO, the material that is actually accumulated, through the reaction enthalpy and the molar mass of CaO ($M_{CaO} = 56.077$ g/mol):

$$q_{CaO} = \frac{\Delta H_r}{M_{CaO}} = \frac{104.4}{0.056077} = 1861.7\ \mathrm{kJ/kg} = 0.5171\ \mathrm{kWh/kg}$$

Each kilogram of hydrated calcium oxide therefore returns about 0.52 kWh, and this figure links the energy demand to the mass to be stored.

3.5.2) Design basis and energy to be stored

The storage is sized on the winter design day, for which the daily energy to be delivered is 605.7 MWh. Two scenarios are considered. Scenario A is quasi-autonomous: its capacity sustains the full district demand for four days and, by lowering the delivered load to 80 % during prolonged periods of low solar production, the same stored energy is stretched to cover five days; the grid is called upon only on the few critical days on which the store is finally exhausted. Scenario B keeps the grid as a systematic back-up and is sized for two days at full coverage. The energy to store is the daily demand times the days of autonomy and the coverage:

$$E_{storage} = E_{day} \cdot n_{days} \cdot c$$

Scenario	Daily demand [MWh]	Days	Coverage	E_storage [MWh]
A (quasi-autonomous)	605.7	5	80 %	2422.8
B (grid-assisted)	605.7	2	100 %	1211.4

The autonomy of Scenario A is obtained at the cost of about twice the stored energy of Scenario B.

3.5.3) Material masses

The mass of calcium oxide is the energy to store divided by the specific energy, while the masses of hydroxide and water are fixed by the stoichiometry through the molar-mass ratios:

$$m_{CaO} = \frac{E_{storage}}{q_{CaO}} \qquad \frac{m_{Ca(OH)_2}}{m_{CaO}} = 1.3213 \qquad \frac{m_{H_2O}}{m_{CaO}} = 0.3213$$

Material	Ratio to CaO	Scenario A [t]	Scenario B [t]
CaO	1.0000	4684.9	2342.5
$Ca(OH)_2$	1.3213	6190.0	3095.0
H_2O	0.3213	1505.1	752.5

The hydroxide is the heaviest material and sets the size of the largest vessel.

3.5.4) Volumes and silo geometry

The material volume comes from the bulk density, and the silo volume adds the freeboard through the fill factor $f = 0.85$:

$$V_{mat} = \frac{m}{\rho} \qquad V_{silo} = \frac{V_{mat}}{f}$$

The bulk densities are 400 kg/m^3 for the CaO powder, 500 kg/m^3 for the hydrated lime and 1000 kg/m^3 for the water. The silos are vertical cylinders with aspect ratio $H/D = 1.5$, from which the diameter and height of a single unit are

$$D = \left(\frac{4\,V_{unit}}{\pi\,(H/D)}\right)^{1/3} \qquad H = (H/D)\cdot D$$

The inventory is split into identical units of a standard size, which simplifies construction and allows part of the storage to be isolated for maintenance. In ideal terms this gives four CaO silos and four $Ca(OH)_2$ silos in Scenario A, and two of each in Scenario B, plus one water tank in both cases; the counts that account for the real losses of the process are given in Section 3.6.5.

Scenario A — full autonomy

Vessel	Material vol. [m^3]	Silo vol. [m^3]	N	D [m]	H [m]
CaO silos	11712	13779	4	14.30	21.45
$Ca(OH)_2$ silos	12380	14565	4	14.57	21.85
H_2O tank	1505	1771	1	11.45	17.18

Scenario B — grid-assisted

Vessel	Material vol. [m^3]	Silo vol. [m^3]	N	D [m]	H [m]
CaO silos	5856	6890	2	14.30	21.45
$Ca(OH)_2$ silos	6190	7282	2	14.57	21.85
H_2O tank	753	885	1	9.09	13.64

The oxide and hydroxide silos are never full at the same time, since the calcium is held in one state or the other; sizing each for its full inventory is a conservative choice that lets the loop work at any state of charge.

3.5.5) Loss factors and corrected sizing

The masses above assume a complete reaction and full heat delivery. Two real effects increase the material to install: an incomplete conversion X (0.80–0.95), because not all the oxide hydrates within the residence time and the material loses reactivity over cycles, and a reactor thermal efficiency η_{th} (0.85–0.95), accounting for wall losses and imperfect sensible-heat recovery. Including them, the required oxide mass becomes

$$m_{CaO} = \frac{E_{storage}}{X \cdot \eta_{th} \cdot q_{CaO}}$$

The two coefficients are not known with precision at this stage of the design, so the sizing is carried out for a range of values. The conservative combination (X = 0.80, η_th = 0.85) multiplies the energy basis by about 1.47, while the optimistic one (X = 0.95, η_th = 0.95) multiplies it by only 1.11. The design value adopted in this work is the intermediate combination X = 0.875 and η_th = 0.90, which raises the energy basis by a factor 1.27 and gives a realistic estimate of the inventory.

Vessel	Mass [t]	Silo vol. [m^3]	N	D [m]	H [m]
CaO silos	5 949.1	17 497	5	14.38	21.56
$Ca(OH)_2$ silos	7 860.3	18 495	6	13.78	20.67
H_2O tank	1 911.2	2 248	1	12.40	18.61

The strong dependence on these two coefficients shows how much the reactor design and the heat recovery affect the size of the storage. The value of η_th is here estimated from the literature on gas–solid thermochemical reactors, and its influence on the final size of the plant is quantified in the economic scenarios of Chapter 6.

3.5.6) Summary

With the design values adopted above, the storage of Scenario A holds 5949 tonn of calcium oxide, 7860 tonn of calcium hydroxide and 1911 tonn of water, for a total silo volume of 38241 m^3. The inventory is distributed over five CaO silos (Ø 14.38 m × 21.56 m), six $Ca(OH)_2$ silos (Ø 13.78 m × 20.67 m) and one water tank (Ø 12.40 m × 18.61 m), that is twelve vessels in all. Scenario B holds 2975 tonn of oxide, 3930 tonn of hydroxide and 956 tonn of water, for 19120 m^3 distributed over three CaO silos (Ø 13.53 m × 20.29 m), three $Ca(OH)_2$ silos (Ø 13.78 m × 20.67 m) and one water tank (Ø 9.85 m × 14.77 m), seven vessels in all. The larger number of hydroxide silos reflects the fact that the hydrated form is the heavier of the two solids. The sizing parameters are collected below.

Symbol	Meaning	Value
q_CaO	Specific reaction energy of CaO	0.5171 kWh/kg
ρ_CaO	Bulk density, CaO powder	400 kg/m^3
ρ_$Ca(OH)_2$	Bulk density, $Ca(OH)_2$ powder	500 kg/m^3
ρ_H_2O	Density, liquid water	1000 kg/m^3

Symbol	Meaning	Value
f	Silo fill factor	0.85
H/D	Silo aspect ratio	1.5
X	Conversion	0.875 (design value; range 0.80–0.95)
η_th	Reactor thermal efficiency	0.90 (design value; range 0.85–0.95)

3.6) Solar field sizing

The solar field closes the calculation chain, since during the hours of sunlight it must provide both the power that serves the live demand and the power that charges the storage for the dark hours. The field is sized on a clear-sky winter design day, the condition in which the demand is highest and the solar resource weakest: if the field can charge the storage on that day, it can do so on any other day of the year.
The thermal power required at the receiver is the sum of these two contributions, the second set by the energy to be stored and the daily window of useful sunlight t_{sun}:

$$Q_{rec} = Q_{live} + Q_{charge} \qquad Q_{charge} = \frac{E_{storage}}{t_{sun}}$$

The ratio of this power to the one absorbed by the block at nominal conditions defines the solar multiple, $SM = Q_{rec}/Q_{pb}$, which measures how much the field is oversized to charge the storage while still serving the load. The reflective area needed to collect Q_{rec} follows from the design irradiance and the efficiency chain that links the radiation on the field to the heat delivered at the receiver:

$$A_{field} = \frac{Q_{rec}}{DNI \cdot \eta_{opt} \cdot \eta_{rec}} \qquad N_h = \frac{A_{field}}{a_h}$$

where DNI is the design direct normal irradiance, η_opt the optical efficiency of the field (cosine, shading, blocking, reflectivity and attenuation losses), η_rec the receiver thermal efficiency and A_h the unit mirror area. The land area follows from a ground-coverage ratio and the tower height from the size of the field, both taken from existing central-receiver plants used as a reference. The same solar field is adopted for both scenarios, so that the comparison between them isolates the effect of the storage strategy alone.

The design point is set on 4 January, the clear-sky day on which the winter demand and the low solar altitude combine most unfavourably. The design direct normal irradiance is DNI = 850 W/m^2, the optical efficiency of the field is η_opt = 0.60, accounting for cosine, shading, blocking, reflectivity and atmospheric attenuation losses, and the receiver efficiency is η_rec = 0.88, accounting for radiative and convective losses at the aperture. With about 9.4 equivalent hours of full-power sunlight on the design day, and with an oversize factor of 1.2 applied to guarantee the charge of the storage under the design condition, the required receiver power and mirror area follow from the equations above.

The resulting solar field consists of a heliostat mirror area of 256884 m^2, about 257000m^2, feeding a central receiver of 115.3 MWth design power. The receiver can therefore deliver up to 1084 MWh of heat per day, against the 605.7 MWh required by the district on the winter design day: the margin is what allows the storage to be charged while the live demand is served.

3.7) Plant-level energy balance and sizing summary

This closing section assembles the previous results into a plant-wide energy balance and a sizing summary for the two scenarios, verifying that the calculation chain is consistent from the solar energy collected by the field down to the services delivered to the district. The balance traces each unit of solar energy along its path: the radiation on the field, reduced by the optical and receiver losses to the heat at the receiver; the split of this heat between the live demand and the charging of the storage; the return of the stored energy during the dark hours, with the round-trip losses of the reaction and the heat recovery; and the final conversion by the trigeneration block into electricity, heat and cooling. The overall performance is summarised by a plant-level efficiency, the ratio of the useful energy delivered to the district to the solar energy incident on the field:

$$\boldsymbol{\eta_{global}} = \frac{\boldsymbol{E_{el} + E_{heat} + E_{cool}}}{\boldsymbol{E_{solar}}}$$

A key consistency check is the closure of the storage over the daily cycle: the energy charged during sunlight must equal the energy discharged during the dark hours, once losses are included. On the winter design day the receiver collects up to 1084 MWh, of which 605.7 MWh are required by the district, so that the surplus is available to charge the store; over the year the daily balance between charging and discharging is resolved by the operational model of Chapter 4, which follows the state of charge of the storage day by day. The main sized quantities of every section are collected in the summary table below, and they constitute the reference configuration on which the operational analysis of Chapter 4 and the comparative study of Chapter 5 are built.

Quantity	Scenario A	Scenario B
Heliostat mirror area	256 884 m^2	(same)

Receiver design power	115.3 MWth	(same)
Receiver daily capacity	1084 MWh/day	(same)
Steam turbine	10 MWe, extraction	(same)
Thermal power to turbine	27.8 MWth	(same)
District-heating interface	22.9 MWth	(same)
Absorption chiller	13.7 MW cooling	(same)
Winter design-day energy	605.7 MWh/day	(same)
Days of autonomy	5 (at 80 % coverage)	2 (at 100 %)
Ideal storage capacity	2 422.8 MWh	1 211.4 MWh
Installed storage capacity	3 076.6 MWh	1 538.3 MWh
CaO inventory	5 949 t	2 975 t
$Ca(OH)_2$ inventory	7 860 t	3 930 t
H_2O inventory	1 911 t	956 t
Silos (CaO + $Ca(OH)_2$ + H_2O)	5 + 6 + 1 = 12	3 + 3 + 1 = 7
Total silo volume	38241 m^3	19120 m^3
Max discharge power	50.7 MWth	(same)

Table 3.1 Sizing summary of the plant for the two scenarios.

4) OPERATIONAL ANALYSIS

4.1) Power block model

The power block is a steam Rankine cycle, modelled in DWSIM with the IAPWS-IF97 steam tables. It is built around a 10 MW_e steam turbine of the Siemens SST-200 class, fed with live steam at 90 bar and 540 °C and condensing at 0.10 bar. The same machine is analysed in three modes: a base configuration producing only electricity, a winter configuration with a single extraction feeding the heat demand (space heating and DHW) , and a summer configuration with two extractions feeding the absorption chiller and the domestic hot water (trigeneration). The three modes share the same live-steam conditions and the same nominal mass flow and differ only in where steam is bled from the turbine, which is the mechanism that couples the electrical output to the thermal demand of the district.

4.1.1) Base configuration (electricity only)

In the base configuration the whole steam flow expands from the turbine inlet to the condenser, with no extraction. The design parameters are listed below.

Parameter	Symbol	Value	Unit
Turbine inlet pressure	P_1	90	bar
Live steam temperature	T_3	540	°C
Condensing pressure	P_c	0.10	bar
Turbine isentropic efficiency	η_t	0.88	–
Pump isentropic efficiency	η_p	0.80	–
Generator efficiency	η_g	0.97	–
Nominal steam mass flow	$\dot{m}$	8.84	kg/s

The cycle is closed by a single feedwater pump; no regeneration is included, in keeping with the modest size of the plant. The resulting thermodynamic states are summarised below.

Stream	Description	T [°C]	P [bar]	h [kJ/kg]	x
S1	Condensate (sat. liquid)	45.8	0.10	191.8	0
S2	Feedwater (pump outlet)	46.7	90	203.2	liq.
S3	Live steam (turbine inlet)	540	90	3487.2	1

Stream	Description	T [°C]	P [bar]	h [kJ/kg]	x
S4	Turbine exhaust (to condenser)	45.8	0.10	2309.8	0.885

The net electrical power delivered to the users is the mechanical power of the turbine reduced by the generator and auxiliary losses and by the pump consumption,

$$W_{el,net} = W_t \, \eta_g - W_p$$

and the nominal flow of 8.84 kg/s delivers exactly 10.0 MW_e. The thermodynamic efficiency of the cycle,

$$\eta_{cycle} = \frac{W_t - W_p}{Q_{in}} = 0.355$$

reproduces the design value (0.36) within 1.4%, while the net electrical efficiency referred to the heat supplied to the steam generator is η_el = 0.344. The turbine exhaust quality is 0.885, above the 0.88 limit usually adopted to avoid blade erosion. The heat supplied to the cycle is 29.0 MW_{th} and the heat rejected at the condenser 18.7 MW_{th}; the small excess on the former with respect to the preliminary sizing (+4.5%) reflects the fact that the mass flow also covers the generator losses.

4.1.2) Cogeneration and the extraction coefficient β

When steam is extracted upstream of the condenser to feed a thermal user, that steam no longer expands through the remaining stages, so the turbine produces less electricity. The trade-off is captured by a single coefficient, β, defined as the electrical power lost per unit of heat delivered to the user,

$$\beta = \frac{\Delta W_{el,lost}}{Q_{th}} = \frac{\dot{m}_{ext} \, (h_{ext} - h_{cond}) \, \eta_g}{Q_{th}}$$

where the numerator is the work the extracted steam would have produced expanding down to the condenser. Since β depends only on the extraction pressure and the cycle efficiencies, and not on the extracted flow, it is an intensive property of each extraction point. It provides a compact linear cogeneration model: the heat the cycle must receive to satisfy a given electrical and thermal demand is

$$Q_{in} = \frac{W_{el} + \beta\, Q_{th}}{\eta_t\, \eta_g}$$

which is the relation used throughout the seasonal dispatch analysis of the following sections.

Winter mode - district-heating and DHW extraction

In winter a single extraction at 2 bar feeds the district-heating network, sized on an 80 °C supply / 60 °C return, with the extracted steam condensing and subcooling to 70 °C. Evaluating the lost-work expression at this pressure gives β = 0.17 on a latent-heat basis, or 0.159 if the sensible subcooling heat is also credited to the user. The first value is the one adopted for the dispatch, as a conservative estimate. In this mode the turbine follows the electrical load and the extraction is set by the heating demand, so its electrical output is not fixed but varies with the season.

Summer mode - trigeneration

In summer the machine works in trigeneration, with two simultaneous extractions: one at 8 bar feeding the double-effect absorption chiller, and one at 2 bar feeding the domestic hot water. The 8 bar steam desuperheats and condenses to saturated liquid at 170 °C, the temperature the double-effect chiller requires; the 2 bar steam is subcooled to 70 °C as in winter. The two extraction coefficients are β_chiller = 0.277 and β_DHW = 0.159.

With the flows sized on the summer demand, 4.85 kg/s to the chiller and 2.36 kg/s to the domestic hot water, the block delivers simultaneously about 6.4 MW$_e$, 10.6 MW$_{th}$ of heat to the chiller and 5.6 MW$_{th}$ to the hot water. The cooling produced follows from the chiller coefficient of performance,

$$Q_{cool} = COP \cdot Q_{chiller} = 1.3 \times 10.6 \approx 13.8 \text{ MW}$$

The net electrical output of 6.4 MW$_e$ still exceeds the average summer electrical demand of 4.45 MW$_e$, so in this mode the plant covers cooling, hot water and electricity at the same time, with no competition between the users for the available steam.

Summary of the three modes

The three operating modes are compared below. All of them close their mass and energy balances exactly in DWSIM and reproduce the preliminary sizing within a few per cent; together they provide the operating points, electrical output, thermal duties and the β coefficients, that feed the seasonal dispatch analysis of the next sections.

Quantity	Base	Winter extraction	Summer trigeneration
Extraction pressure	none	2 bar	8 bar + 2 bar
Thermal users	–	district heating + DHW	chiller + DHW
Net electrical power	10.0 MW	load-following	6.4 MW
Heat to chiller	–	–	10.6 MW
Heat to DHW / DH	–	district heating	5.6 MW
Cooling produced	–	–	13.8 MW
Extraction coefficient β	–	0.17	0.277 / 0.159

4.2) Dispatch strategy and operating logic

The plant must decide, hour by hour, what to do with the heat produced by the solar field, comparing it with what the district is asking for. What makes this plant different from a conventional cogeneration unit is that the demand has two distinct outcomes electricity and heat, and that the storage can serve them through two separate outputs. As will be seen, this is what allows both to be met even at the moments of highest load.

4..2.1) How the heat is routed: the two outputs of the storage

The solar field collects heat only during sun hours; the district asks for electricity, heating or cooling and hot water around the clock. The thermochemical storage bridges this gap in time: it is charged with the surplus solar heat during the day, dehydrating the calcium hydroxide, and discharged at night, rehydrating the calcium oxide and returning the stored heat when the sun is gone.

The stored heat, released at high temperature by the hydration reaction, can leave the storage through two paths. Through the first output it feeds the steam generator and drives the turbine, producing electricity. Through the second output it is sent directly to a heat exchanger that serves the thermal users, district heating in winter, the absorption chiller in summer, and the domestic hot water, without passing through the turbine at all, that's happen when the eletrical power needed is close to the nominal output of the turbine and there isn't the possibility for the spillage.

Heat flow in the plant: the storage feeds the turbine through one output and the thermal users directly through a second one.

4.2.2) Covering the demand: extraction or direct heat

Heat for the thermal users can be supplied in two ways. The first is by extraction (spillage) in which steam is bled from the turbine at an intermediate pressure and gives up its heat to the users. This is efficient, because the steam has already produced work before releasing its heat (it is genuine cogeneration), but it carries a cost: every unit of heat extracted is a unit of electricity the turbine no longer produces, the penalty measured by the coefficient β of Section 4.1.

The difficulty appears at the peak hours. On the winter design day the electrical and the heating peaks coincide at 19:00, when the district asks for 8.9 MW_e and 17.3 MW_{th} at the same time. If that heat were taken by extraction, the turbine could not deliver the 8.9 MW_e to the users and the peak would simply be unfeasible.

This is the reason for the second, direct output of the storage. At the peak the turbine is left free to produce only the electricity required, while the heat is supplied straight from the storage through the heat exchanger, with no penalty on the electrical side. The two routes are therefore used according to the margin available: extraction when the turbine has spare capacity, because it is the more efficient of the two; the direct output when the electrical peak would otherwise saturate the machine. In this way the plant can meet the electrical and the thermal peak at the same instant, which a single turbine alone could not do.

4.2.3) Charging the storage, and producing beyond the demand

Once the instantaneous demand, electrical and thermal has been covered, whatever the field still collects is charged into the storage, which fills up through the sunny hours.

In summer a further situation arises: the field collects much more than the district needs, and the storage, after a few hours, is full. The surplus heat must then be rejected by defocusing part of the heliostat field: the mirrors are steered away from the receiver, so that the corresponding solar radiation is simply not collected and the thermal input to the plant is reduced. Defocusing is the standard curtailment practice of central-receiver plants, and it involves no dissipation of heat already collected but a deliberate reduction of the collection itself. Throughout this work, the "defocused energy" denotes the solar energy discarded in this way. To limit this loss the turbine is not kept tied to the local demand: when surplus heat is available and the store is full, the machine is pushed up to its nominal operating condition and the additional electricity is exported to the grid. Only what exceeds even this, when the turbine is already at full load, is finally defocused. This strategy, and the option of a second turbine to enlarge the exportable share, are developed in chapter 5.

The priority of the dispatch is therefore clear and always the same: cover the district demand first, charge the storage second, export electricity to the grid third, and defocus only as a last possibility to ensure a costant supply during winter and reduce the loss when the production is higher.

4.2.4) State of charge

All of this is followed through a single quantity, the state of charge of the storage, the heat chemically stored at a given hour, equivalently the mass of charged calcium oxide ready to react. It rises when the store is charged and falls when it is discharged,

$$SoC(t) = SoC(t-1) + (\,\text{charged} - \text{discharged}\,)$$

and is bounded between a small safety reserve and the installed capacity, the latter set by the days of autonomy defined in the sizing. A few physical limits close the picture: the receiver cannot collect more than its 115.3 MWth rating, the discharge reactor cannot deliver more than about 50 MWth, and the storage can be neither filled above its capacity nor emptied below its reserve.

4.3) Winter design day: hourly profile

The logic described in Section 4.2 is now applied to the winter design day, the day of highest demand and lowest solar production, on which the plant is sized, to follow the heat hour by hour and to verify that the daily balance closes on the figure adopted for the sizing.
The hourly heat balance is shown below. The demand stays close to 25 MW for most of the day and rises in the evening, when the heating and the electrical loads peak together. The field, on the other hand, collects nothing until 08:00, climbs to a midday maximum of about 114 MW, just below the 115.3 MWth rating of the receiver, and falls back to zero after 17:00. The area between the two curves in the central hours is the surplus heat sent to the storage; in the early morning and through the evening and night, when the field produces little or nothing, the demand is met entirely by discharging the store.

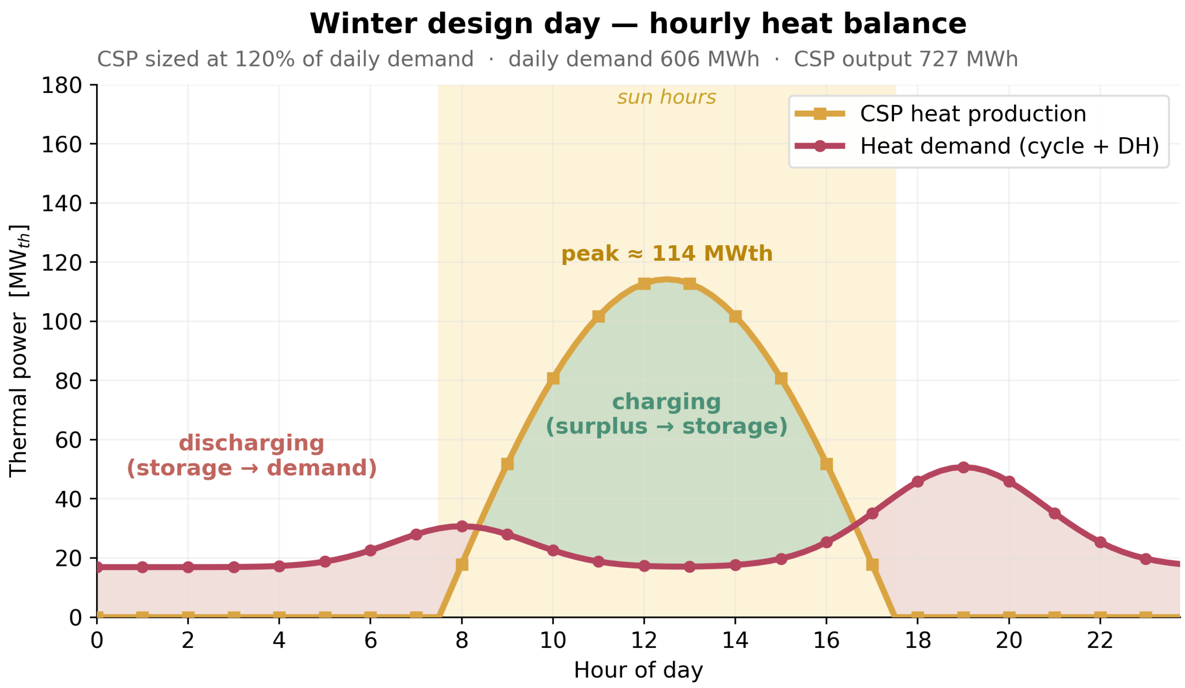

Figure 4.1 Winter design day: hourly heat demand and CSP production

The store is drawn down through the night to cover the demand, reaches its lowest point in the early morning, then fills rapidly once the sun rises, with the charging power approaching the receiver rating around noon. In the evening it discharges again to meet the combined heating and electrical peak, the discharge reaching the design value of about 50 MW.

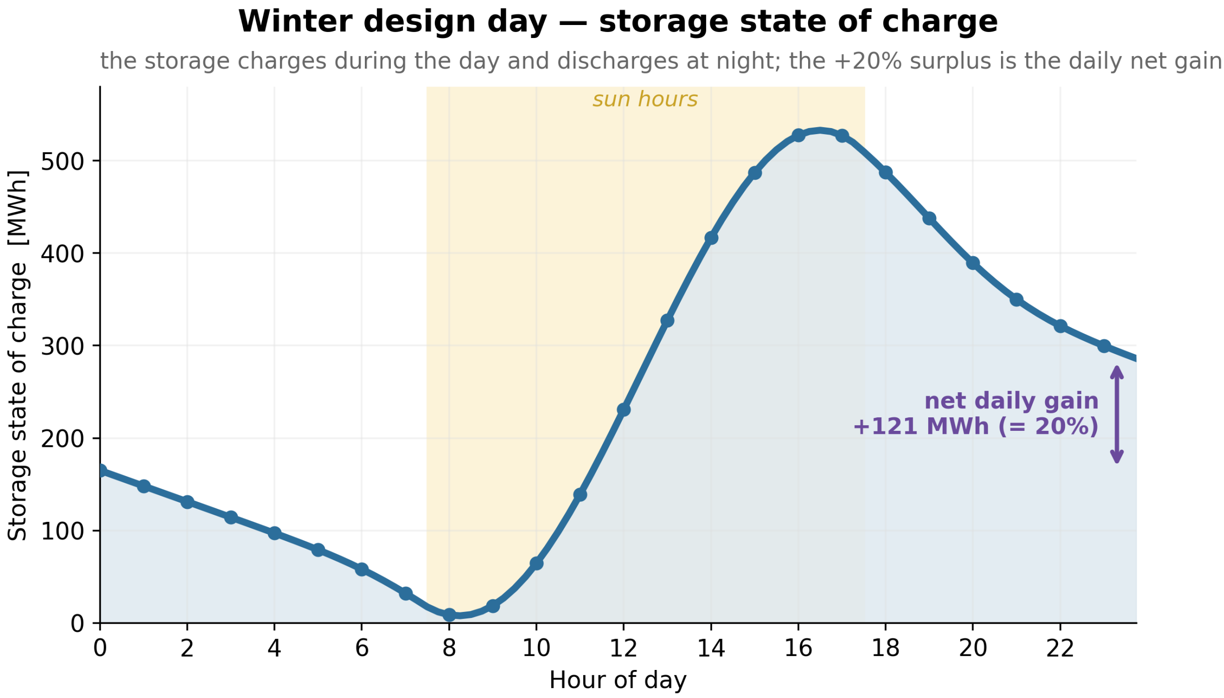

Figure 4.2 Winter design day: storage state of charge over 24 hours

Crucially, the state of charge does not return to its starting value: it ends the day about 121 MWh higher than it began. This is the daily surplus that rebuilds the multi-day reserve, and it follows directly from sizing the field to collect 20% more than the daily demand.

Integrated over the 24 hours, the figures close on the values used for the sizing, as summarised below. The demand adds up to 605.7 MWh, the baseline on which the storage was dimensioned, while the field collects 726.8 MWh, the 20% margin leaving 121.1 MWh in the store at the end of the day. The agreement between the hour-by-hour dispatch and the static design figure confirms that the two are consistent: the operating model reproduces the sizing baseline rather than assuming it.

Daily balance — winter design day	Energy [MWh]
CSP heat collected	726.8
District demand covered	605.7
Surplus stored (reserve build-up)	121.1
Intraday storage swing	≈ 540

The same profile also locates the critical instant of the day, the evening peak at 19:00, when the heating and the electrical demands coincide. It is at this point that the second storage output comes into play, supplying the heat directly so that the turbine remains free to meet the electrical load.

4.4) Seasonal modes

The winter design day examined in Section 4.3 is only one extreme of the year. Over the remaining months the plant operates quite differently, because the nature of the district demand changes with the season, from heating in winter, to little more than hot water in the mild months, to cooling in summer, while the solar field, sized on the winter day, collects steadily more heat as the irradiation grows. This section follows that seasonal evolution from the operating side: how the three modes differ, and what they imply for the storage and for the surplus.

4.4.1) The three operating modes

In winter the thermal demand is dominated by space heating, which together with the domestic hot water keeps the heat demand high all day and drives it to its evening peak. The heat is supplied by extraction at 2 bar and, at the peak, by the direct storage output described in Section 4.2. The field, at its weakest of the year, collects only about 20% more than the daily demand, so the surplus is modest and goes entirely into rebuilding the reserve.

In the mid-season the heating is off and the cooling is not yet needed, so the thermal demand falls to little more than the hot water, around 2 MW_{th} on average. The turbine works almost purely electrically, and the field, now collecting far more than this reduced demand requires, produces a large daytime surplus.

In summer the demand changes character again: cooling demand, supplied by the absorption chiller, which together with the hot water is fed by the double extraction at 8 and 2 bar. The net electrical output drops to about 6.4 MW_e, but the field, with the longest days and the strongest irradiation, collects so much heat that it saturates the receiver for several hours around noon, and the surplus becomes very large.

4.4.2) Seasonal comparison

The three modes are compared in the figure below, which shows the heat demand and the CSP production on a typical day of each season, drawn to the same scale. The demand curve is highest and most peaked in winter, collapses to a low, almost flat profile in the mid-season, and recovers a daytime hump in summer with the cooling load. The production curve tells the opposite story: a narrow bell in winter, a wider one in the mid-season, and a broad plateau in summer where the field is clipped at the 115.3 MWth receiver limit, corresponding to a maximum collectable energy of about 1084 MWh per day. The area between the curves, the surplus charged into the storage, grows from a thin sliver in winter to an significant excess in summer.

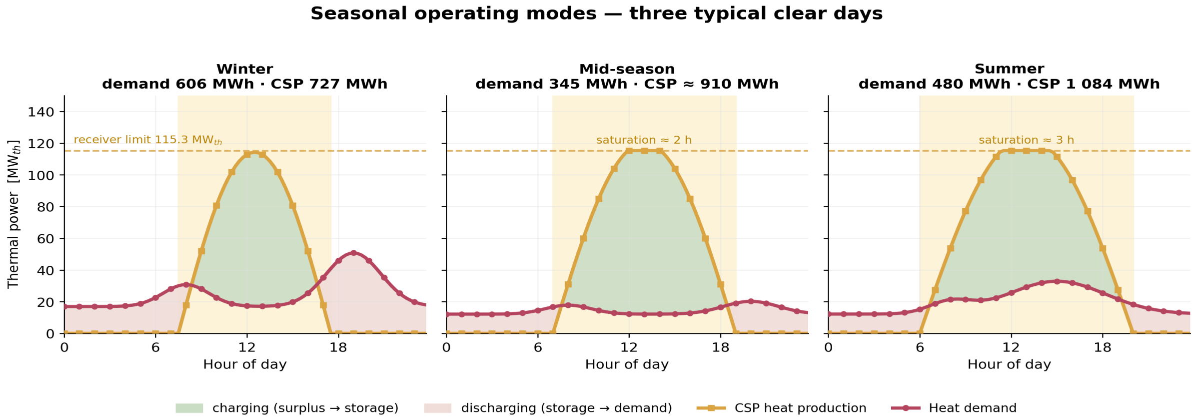

Figure 4.3 Seasonal operating modes: heat demand and CSP production on a typical day of each season.

The daily totals make the trend quantitative: the field collects 727 MWh in winter against a demand of 606, about 744 MWh against 345 in the mid-season, and, in summer, it saturates the receiver at its daily ceiling of roughly 1084 MWh against a demand of only 480. The surplus therefore rises from 121 MWh/day in winter to around 600 MWh/day in summer. Over the year the field collects 256 GWh against a district demand of 139 GWh.

4.4.3) The summer design day in detail

It is worth looking at the summer day with the same detail as the winter one, because it is essentially its mirror image. The hourly balance below shows the field saturated at the receiver limit for about three hours around midday, far above the trigeneration demand; the shaded area is the large surplus that charges the storage until, once the store is full, it can no longer be absorbed.

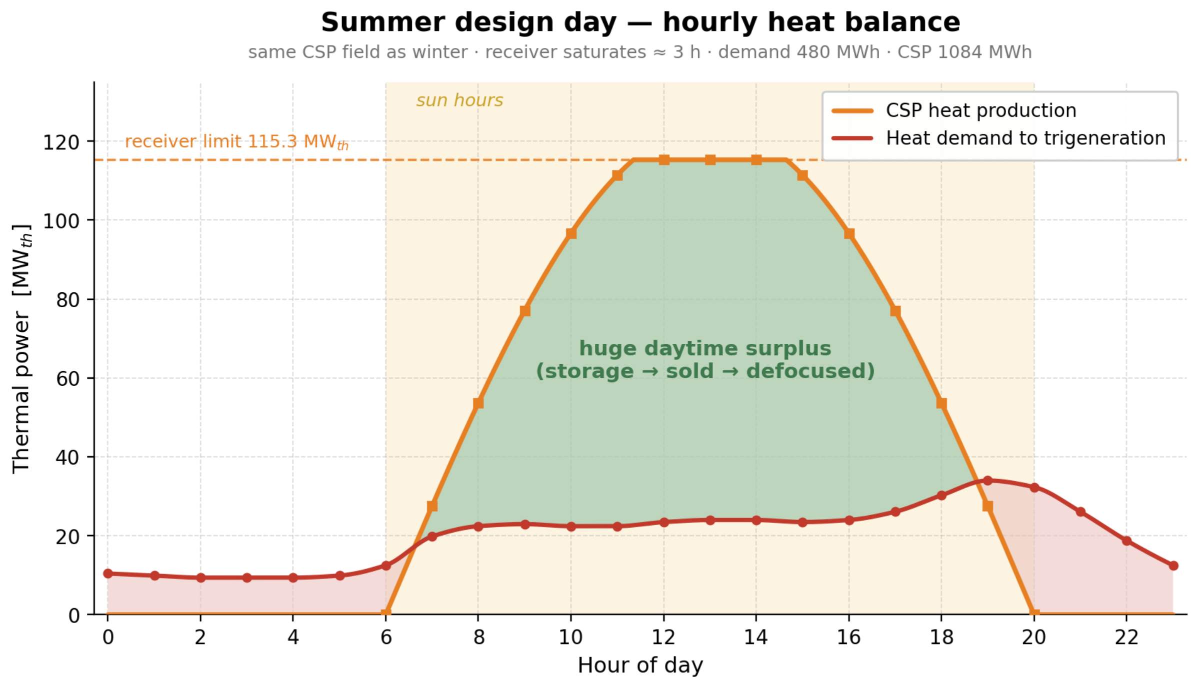

Figure 4.4 Summer design day: hourly heat balance.

The store fills early and completely, then sits at its ceiling for much of the day because no more heat can be absorbed, and that is the visual signature of the summer surplus problem.

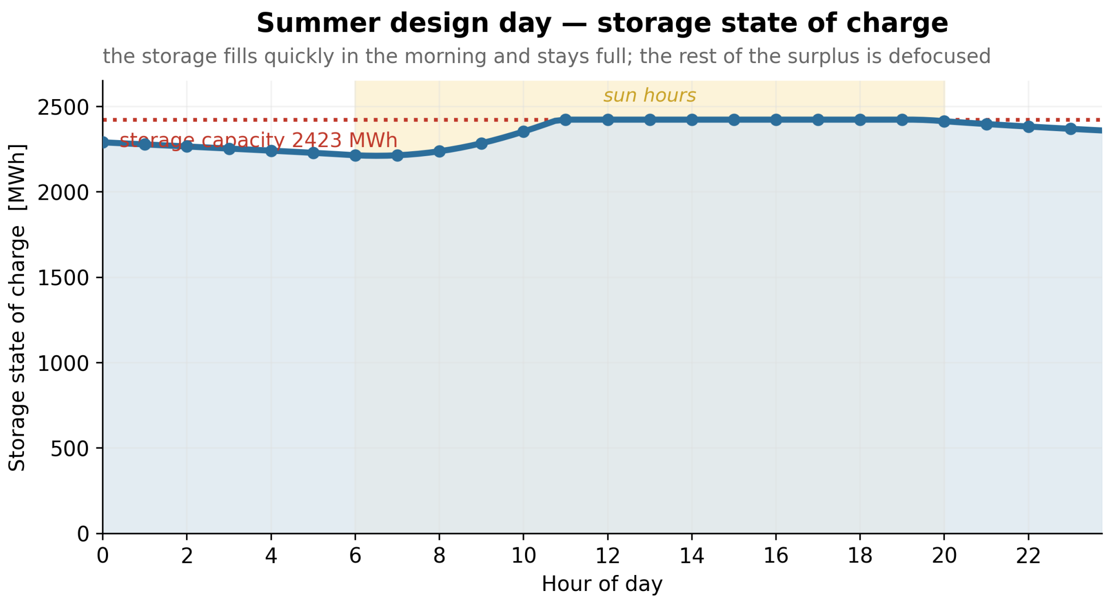

Figure 4.5 Summer design day: storage state of charge over 24 hours.

4.4.4) Summary of the seasonal modes

The same plant, with the same field and the same turbine, covers demands that differ completely in nature across the year; it is the storage and the dispatch logic that absorb these differences. The three modes are summarised below.

Quantity	Winter	Mid-season	Summer
Thermal service	heating + DHW	DHW only	cooling + DHW
Avg. electrical demand	~4.5 MW_e	~4.5 MW_e	~4.5 MW_e
Avg. thermal demand	15.6 MW_{th}	2.2 MW_{th}	9.8 MW_{th}
Extraction pressure	2 bar	minimal	8 + 2 bar
Daily demand / CSP	606 / 727	345 / 744	480 / 1084
Daily surplus	121 MWh	~400 MWh	~600 MWh

4.5) Surplus management and curtailment reduction

During the summer the solar field, which is sized on the winter design day, collects far more heat than the district requires. On the summer design day the trigeneration block draws 480 MWh from the storage, while the field, saturating the receiver, delivers 1 084 MWh: the surplus is about 600 MWh in a single day. Once the district is served and the store is full, this excess can only be defocused, the heliostats are steered off the receiver and the heat is simply not collected. The surplus is structural, since it follows from sizing the field on the worst day of the year, and over the year it amounts to a large share of everything the plant collects.Two ways of reducing this loss are considered. The first, analysed in this section, does not modify the plant: the turbine already installed is operated at full load beyond the local demand, so that a larger share of the available heat is converted and the additional electricity is sold to the grid. The second, which adds a turbine dedicated to the recovery of the surplus, is analysed in the following chapter.

4.5.1) Operating strategy: full-load night-time export

In the base dispatch of Section 4.2 the turbine simply follows the district: it produces the 4.45 MWe the users require, drawing from the storage only the heat needed for that, and everything else the field collects is charged into the store until the store is full. But the machine is rated at 10 MWe, so for most of the summer it runs at less than half of its capability while heat that could have driven it is being thrown away. The alternative is to let the turbine work at its nominal point whenever there is heat that would otherwise be lost: the additional electricity, beyond what the district consumes, is exported to the grid. The turbine is pushed to full load only when the storage is full and the field is still collecting more than the district needs, only when the alternative to burning that heat is defocusing it. In every other condition, and through the winter, the machine keeps

following the local demand, so the reserve built up in the store is never spent to sell electricity. This distinction matters: running the turbine at full load indiscriminately, all year round, would drain the storage in winter and force the plant to import from the grid far more than it does, defeating the purpose of the storage.
The effect on the summer design day is shown below. Drawing heat at the nominal rate of 27.8 MWth instead of the 12.4 MWth required by the local electrical load, the plant takes 857 MWh out of the store over the day instead of 480. The store, being emptied faster, no longer sits at its ceiling for the whole afternoon, and it can therefore absorb a larger share of what the field is collecting.

$$P_{\text{extra}} = P_{\text{turb,max}} - P_{\text{el,demand}} = 10 - 4.45 = 5.55\ \text{MW}_e$$

which draws an additional heat rate from the storage of

$$\dot{Q}_{\text{extra}} = \frac{P_{\text{extra}}}{\eta_t\, \eta_{sg}} = \frac{5.55}{0.36 \times 0.98} \approx 15.7\ \text{MW}_{th}$$

sustained over the whole day, this additional heat rate corresponds to

$$E_{extra} = \dot{Q}_{extra} \cdot \Delta t = 15.7 \times 24 \approx 377\ \text{MWh}_{th}$$

so that the heat drawn from the storage over the day rises from the 480 MWh required by the local demand to

$$E_{drawn} = E_{base} + E_{extra} = 480 + 377 = 857\ \text{MWh}_{th}$$

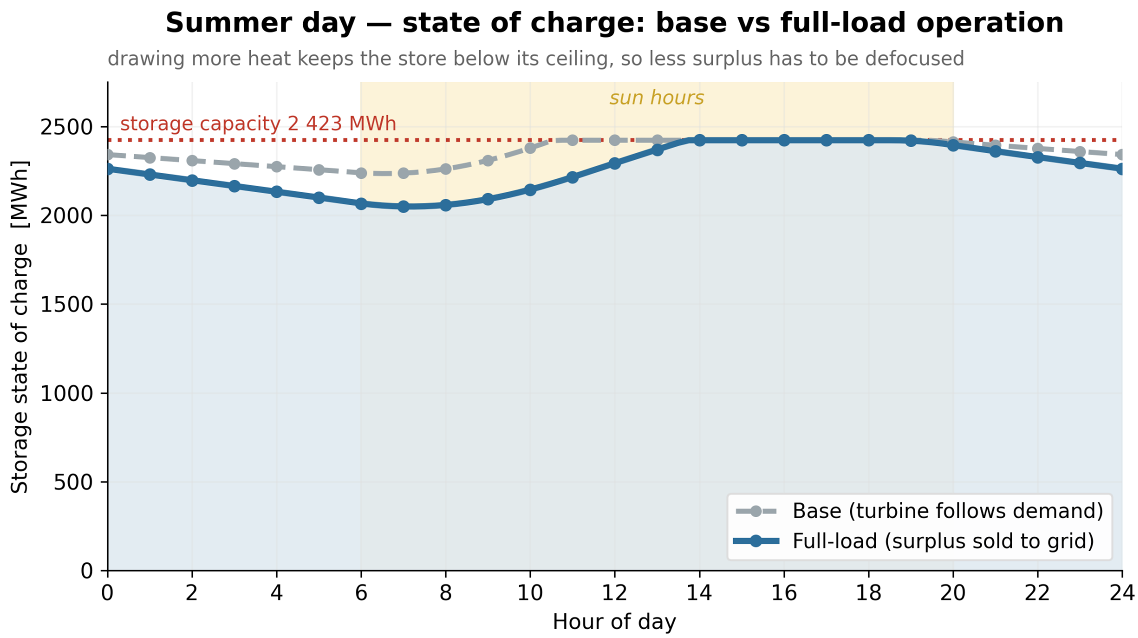

Figure 4.6 Storage state of charge over the summer design day, baseline operation versus full-load export.

The result is a substantial recovery of energy that would otherwise be wasted. On the design day the electricity exported to the grid rises from nothing to 133 MWh, while the defocused heat falls from 547 to 253 MWh, a reduction of about 54 %.

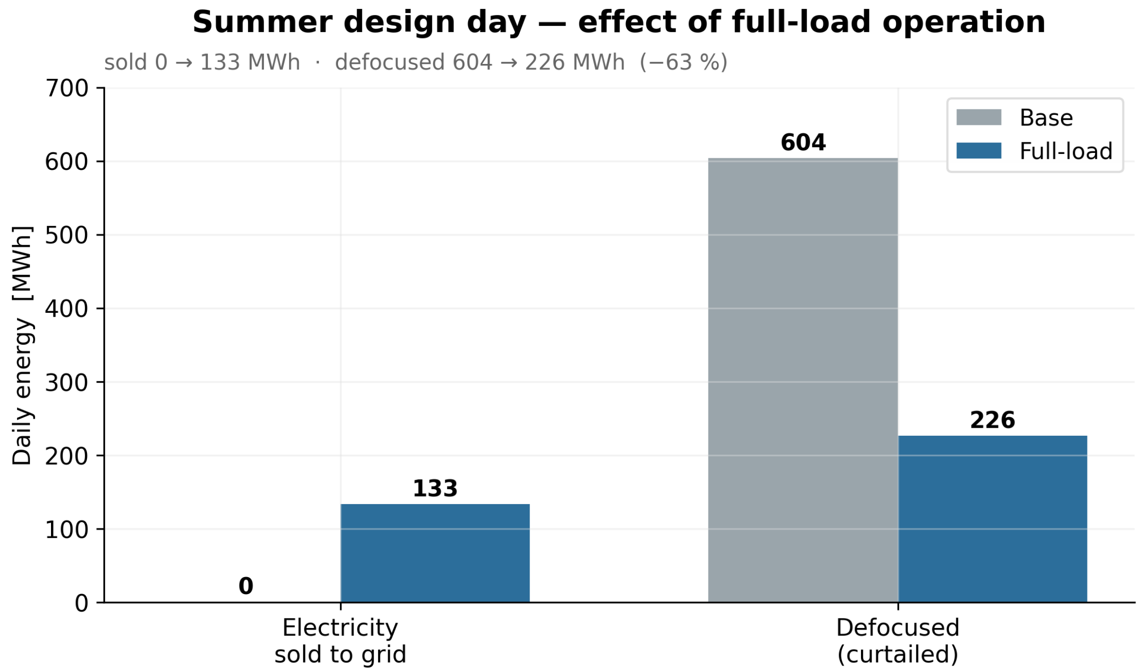

Figure 4.7 Daily electricity sold to the grid and defocused heat, baseline versus full-load night strategy.

Applying the same rule over the whole reference year, and keeping the winter dispatch untouched, the annual defocused heat falls from 123 GWh to about 41 GWh, a reduction of roughly two thirds, and the plant exports 30 GWh of electricity. Crucially, the grid import is unaffected, remaining at 6.4 GWh: the strategy spends only heat that would have been lost anyway, and never the reserve that covers the winter deficit.
This is a purely operational measure, it requires no additional equipment, only a dispatch rule, and it already recovers a large part of the surplus. Yet a third of the defocusing survives it, because a single 10 MWe machine can absorb at most the difference between its rating and the local load: once the turbine is at its nominal point, any further excess has nowhere to go.

4.6) Energy deficit management

The surplus of the warm months has its counterpart in winter. During a prolonged spell of low irradiance the field collects less than the district requires, so that the storage, no longer recharged during the day, is drawn down continuously. The plant then lives on its reserve, and the question is how long that reserve lasts.

The endurance of the store follows directly from its capacity and from the rate at which it is emptied. On the winter design day the district draws 605.7 MWh per day, so a store holding 2423 MWh, the capacity adopted for Scenario A, sustains the full demand for four consecutive days without sun. This is where the management of the storage comes in. On the rare days in which a perturbation persists and the reserve is running low, the load delivered to the district can be temporarily lowered to 80 % of its nominal value: the daily draw falls accordingly, and the same stored energy stretches from four to five days. The measure is occasional and temporary, for the rest of the year the district is served in full, but it buys a day of autonomy at no capital cost, which is precisely the point at which a day is worth most.

Scenario B discharges at full demand and reaches its reserve after two days, beyond which the grid takes over.

Quantity	Scenario A	Scenario B
Storage capacity	2423 MWh	1211 MWh
Strategy in a prolonged deficit	reduce demand to 80%	import from the grid
Winter autonomy	5 days	2 days

The mechanism is illustrated below for a hypothetical sequence of days without sun, in which the store is simply run down from a full charge.

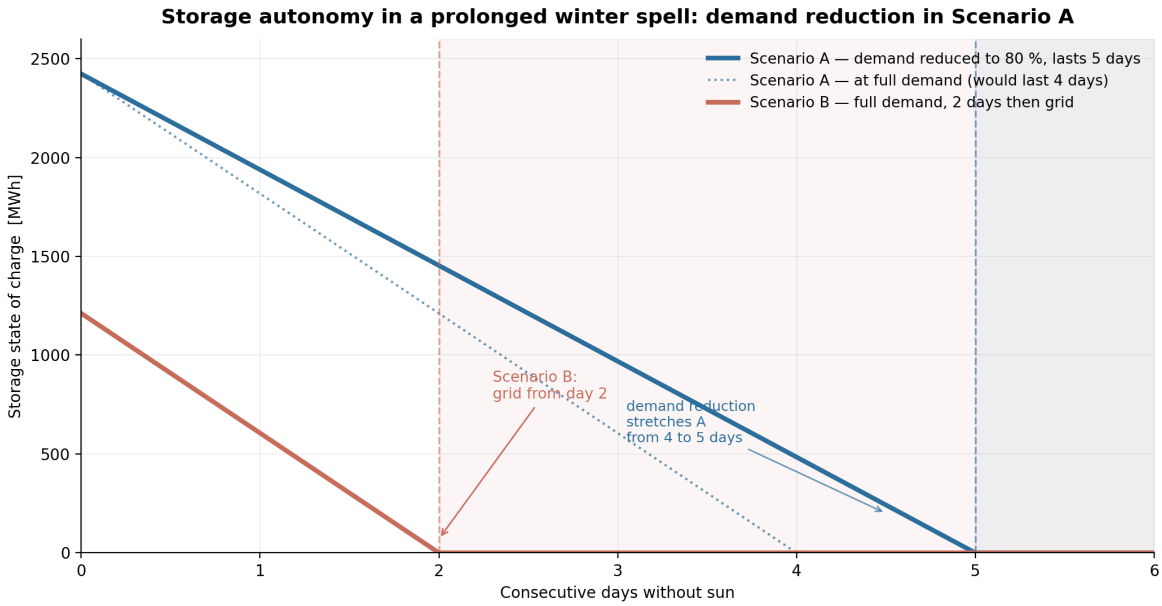

Figure 4.8 Storage depletion during a prolonged winter spell without sun, for the two scenarios

5) COMPARATIVE ANALYSIS AND OPTIMIZATION

5.1) Power-block configuration: single versus dual 10 MW turbine

The operational analysis of Chapter 4 exposed a structural feature of the plant: since the heliostat field is sized on the energy balance of the worst clear-sky winter day (Section 3.7), for most of the year the solar production largely exceeds the district demand. Once the silos are full, this surplus has no destination and must be rejected by defocusing part of the heliostat field. This section quantifies the phenomenon and evaluates a plant-level countermeasure: a second 10 MW steam turbine, operated in pure condensing mode, dedicated to converting the rejected surplus into electricity for grid export. The comparison between the single-turbine and the dual-turbine configuration is carried out on the reference configuration with four silo modules and 80% demand coverage (Scenario A).

5.1.1 The defocusing problem in the single-turbine configuration

In the single-turbine layout the dispatch priority is: district demand first, then charging of the thermochemical storage, and defocusing as the only remaining sink. The daily model shows that the silos, sized for multi-day autonomy rather than for daily cycling, are essentially full from March to October: on an average day the entire surplus is therefore rejected. Over the reference year the defocused energy amounts to 125.8 GWh, to be compared with an annual solar production of 256.1 GWh: 49% of the energy collected by the field is discarded. The monthly distribution (Figure 5.1) shows that the rejection is not a summer-only phenomenon: it starts in March, peaks in July at 20 GWh/month and persists through October, showing the seasonal asymmetry between production and demand.

The paradox highlighted in Section 5.2 completes the picture: the same plant that rejects 126 GWh per year imports 6.4 GWh from the grid in winter. The single-turbine configuration is thus simultaneously over-supplied and grid-dependent, in different seasons.

5.1.2 The dual-turbine configuration

The proposed countermeasure, to avoid the huge amount of defocused energy during the year,is to add a second steam turbine group, identical in rating to the first (10 MW) but operated in pure condensing mode, with no extractions: its only product is electricity, exported to the grid. The dispatch hierarchy is extended by one level:

1. the first turbine follows the district demand, exactly as in the base configuration;
2. the solar surplus charges the silos, up to their capacity;
3. the residual surplus feeds the second turbine;
4. only the energy exceeding the daily absorption capability of the second turbine is defocused.

A key feature of the layout is that the second turbine is not constrained to operate only during sunshine hours. During the day it is fed directly by the receiver; at night it can draw from the silos, which are replenished by the surplus of the following day. The storage therefore acts as a daily buffer that decouples the turbine operation from the solar profile, allowing continuous (24 h) operation whenever enough surplus is available. The daily absorption limit of the second turbine follows from its rating and net efficiency ($\eta_{T2} = 0.36$, equal to the design value of the main cycle):

$$Q_{T2}^{max} = \frac{P_{T2}}{\eta_{T2}} \cdot 24\,\mathrm{h} = \frac{10}{0.36} \times 24 = 667\ \mathrm{MWh/day}$$

It should be noted that the plant requires an operating grid connection in both directions: the second turbine exports the solar surplus, while a limited winter import (6.4 GWh/yr, quantified in Section 5.2) covers the residual deficit when the storage is exhausted. Scenario A should therefore be understood not as an off-grid plant, but as a grid-connected plant with a high degree of self-sufficiency, whose reliance on the grid is minimal on the import side and turns into a net export once the second turbine is added.

5.1.3 Annual energy analysis

Table 5.1 collects the annual results of the daily simulation for the two configurations. The second turbine absorbs 121.2 GWh of thermal energy per year and exports 43.6 GWh of electricity, while the defocused energy collapses from 125.8 to 4.5 GWh (96% reduction). The residual rejection is concentrated in the few summer days in which the surplus exceeds the 667 MWh/day absorption limit.

Quantity	Single turbine	Dual turbine
Annual solar production	256.1 GWh	256.1 GWh
Served district demand	139.0 GWh	139.0 GWh
Defocused energy	125.8 GWh	4.5 GWh
Defocused / production	49%	1.8%
T2 heat input	—	121.2 GWh
T2 electricity export	—	43.6 GWh
T2 operating days	—	269
Days at full absorption	—	80
T2 equivalent full-load hours	—	4,364 h
T2 capacity factor	—	0.50

Quantity	Single turbine	Dual turbine
Winter grid import	6.4 GWh	6.4 GWh

Table 5.1

The exported electricity exceeds the entire annual electric consumption of the district (39.0 GWh): the second turbine more than doubles the electrical output of the plant. Second, a capacity factor of 0.50 (4,364 equivalent full-load hours) is remarkably high for a machine that runs exclusively on energy that would otherwise be wasted; this is a direct consequence of the day/night buffering provided by the silos. Third, the winter grid import is unaffected: the second turbine operates on the surplus and does not interact with the deficit management.
On an annual basis, however, the plant becomes a strong net exporter, selling almost seven times the energy it purchases.
Figure 5.1 compares the monthly defocused energy in the two configurations, and Figure 5.2 shows the monthly profile of the exported electricity: the export follows the solar season, ramping up in March, peaking at 7 GWh/month in July and vanishing in the December–February period, when the whole production is absorbed by the district.

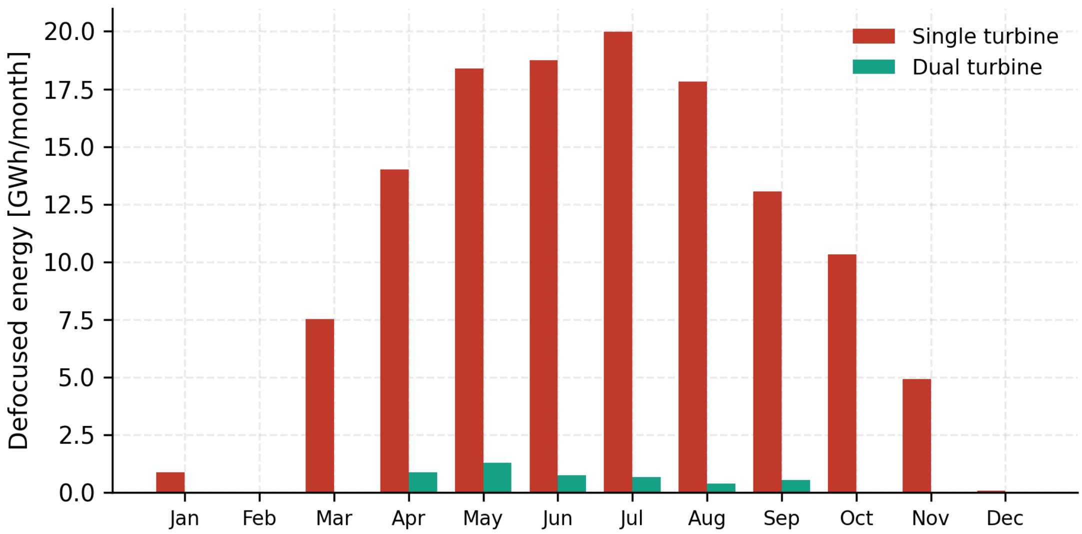

Figure 5.1 Monthly defocused energy in the single-turbine and dual-turbine configurations.

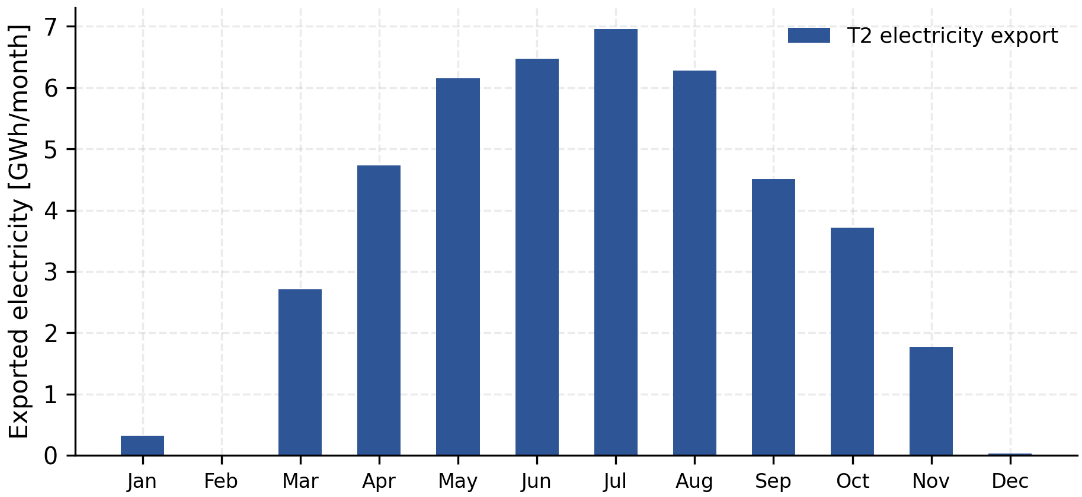

Figure 5.2 Monthly electricity export of the second turbine.

5.1.4 Part-load behaviour

Since the second turbine is fed by a variable surplus, the rate at which solar energy in excess becomes available changes continuously through the year. Figure 5.3 shows the duration curve of the daily heat that reaches the turbine: for about 80 days (667 MWh/day) the surplus saturates the daily absorption limit of the machine, while on the remaining days it is progressively smaller, tapering off towards the winter months when there is no surplus at all.

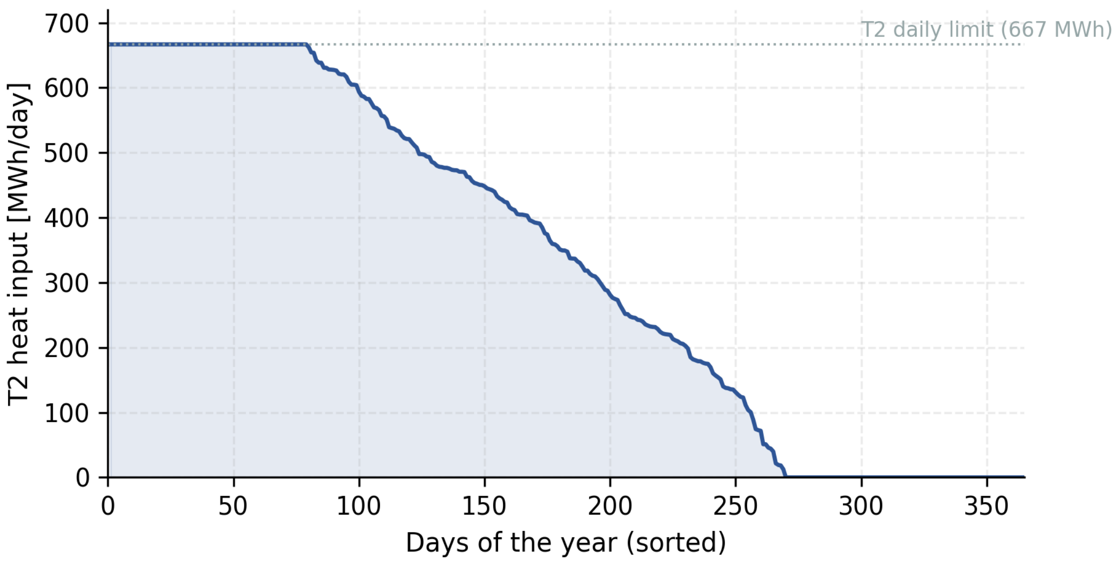

Figure 5.3 Duration curve of the daily heat input to the second turbine

The presence of the thermochemical storage is what allows the turbine to cope with this variability while still operating around its nominal point. Rather than following the instantaneous surplus and running continuously at part load, which for a steam turbine would mean a lower efficiency, the machine draws on the silos as a buffer: the surplus is accumulated and then released to the turbine in blocks at the nominal load, for as many hours as the available energy allows. On a day with little excess heat the turbine therefore runs for fewer hours at full load, instead of many hours at reduced load. This is the operating strategy assumed throughout the analysis, and it is the reason why the annual export of 43.6 GWh reported in Table 5.1 is evaluated at the nominal efficiency of the turbine ($\eta_{T2} = 0.36$): were the machine instead forced to operate at partial load, its efficiency would fall and the exported electricity would be correspondingly lower. The storage thus does more than shift the production in time, it protects the conversion efficiency of the recovery turbine.

5.1.5 Comparison and discussion

Figure 5.4 summarises the comparison as a destination balance of the annual solar production. In the single-turbine configuration nearly half of the collected energy is discarded; in the dual-turbine configuration the same energy stream is split between the district (52%) and the export (47%), with a residual rejection below 2%.

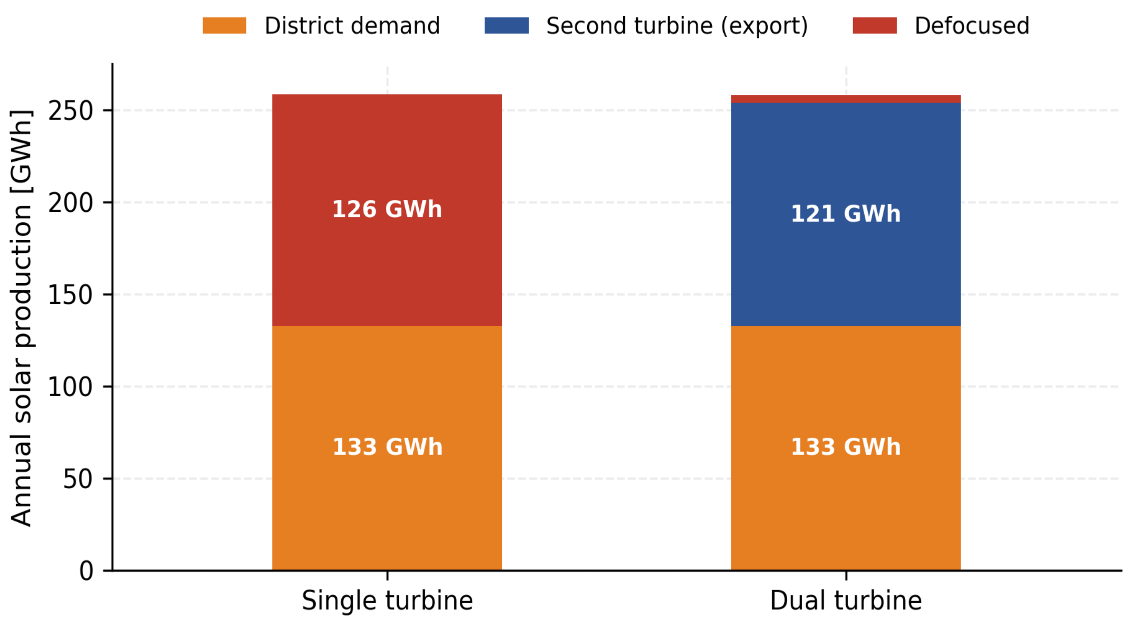

Figure 5.4 Destination of the annual solar production in the two configurations.

The energetic case for the second turbine is compelling, but two qualifications are needed. The first is thermodynamic: in pure condensing mode, 64% of the recovered heat is rejected at the condenser, so the 121 GWh of avoided defocusing become 43.6 GWh of electricity, wasting low temperature heat. The second is economic: the second turbine group essentially doubles the power-block investment, and its revenues depend on the market value of a strongly seasonal, summer-peaked export profile. The trade-off between the additional CAPEX and the export revenues is quantified in Chapter 6.

5.2 Storage autonomy: Scenario A versus Scenario B

The two storage configurations defined in Section 3.6 embody two different design philosophies. Scenario A aims at quasi-autonomous operation: four silo modules provide a nominal capacity of 2,423 MWh. This capacity sustains the full district demand for four days; by lowering the delivered load to 80% during prolonged periods of low solar production, the same stored energy is stretched to cover five days. The extension from four to five days of autonomy therefore comes from the reduced-demand criterion, not from a larger store. Scenario B privileges a smaller and cheaper store: the storage is reduced to two silo modules (1,211 MWh, i.e. two days of average winter demand) and the residual deficits are covered by the grid connection.

A clarification is needed on the coverage factor associated with Scenario A. The 80% figure is not a permanent curtailment of the district services: for most of the year the district receives 100% of its demand, supplied either directly by the solar plant or through the storage. The reduced coverage is a storage-management criterion that applies only during the critical periods, sequences of overcast days with the store already running low, in which the delivered load is temporarily lowered to 80% so as to stretch the available energy and extend the autonomy from four to five days. Outside these rare episodes the coverage is full, and when the store is finally exhausted the missing energy is imported from the grid, so that the district is served in any case. The autonomy of each configuration is defined on this basis, from its capacity and the coverage factor applied in the critical periods:

$$\boldsymbol{t_{aut}} = \frac{\boldsymbol{C_{TCES}}}{\boldsymbol{f_{cov} \cdot Q_{d,w}}} \quad \Rightarrow \quad \boldsymbol{t_{aut,A}} = \frac{\mathbf{2,423}}{\mathbf{0.8 \times 605.7}} = \mathbf{5.0\ days}$$

$$\boldsymbol{t_{aut,B}} = \frac{\mathbf{1,211}}{\mathbf{1.0 \times 605.7}} = \mathbf{2.0\ days}$$

In this section the two configurations are compared on operational grounds, using the daily-resolved model of Chapter 4. To isolate the effect of the storage strategy, both scenarios share the same solar plant, sized in Section 3.7 (257,000 m^2 of mirrors, 115.3 MWth receiver); they differ only in the storage capacity and in the management criterion applied on the critical days. Table 5.2 summarizes the two configurations.

Quantity	Scenario A	Scenario B
Silo modules	4	2
TCES capacity	2,423 MWh	1,211 MWh
Coverage on critical days	0.80	1.00
Nominal autonomy	5.0 days	2.0 days
Heliostat field / receiver	257,000 m^2 / 115.3 MWth	same

Table 5.2

5.2.1 Annual operational results

The daily simulation over the reference meteorological year produces the results collected in Table 5.3. The headline figure is the grid dependence: Scenario B imports 18.9 GWh of heat-equivalent energy per year, against 6.4 GWh for Scenario A. The number of days in which the plant must resort to the grid follows the same pattern: 61 days per year for Scenario B against 28 for Scenario A.

Quantity	Scenario A	Scenario B
Annual grid import	6.4 GWh	18.9 GWh
Days with grid import	28	61
Days with storage discharge	42	36
Average state of charge	82.7%	77.2%
Annual defocused energy	125.8 GWh	102.5 GWh

Table 5.3

Two effects combine to produce the reduction of the import in Scenario A. The first is the larger storage: with twice the capacity, Scenario A rides through the multi-day overcast sequences that exhaust the two silos of Scenario B. The second is the management criterion: temporarily lowering the delivered load to 80% on the critical days stretches the stored energy further, so that the store is depleted less often. The combination of the two is what allows Scenario A to reach the grid on only 28 days a year against the 61 of Scenario B.

Figure 5.5 shows the state of charge of the storage over the year for both scenarios. The behavior is strongly seasonal: from March to October the silos remain essentially full and are cycled only occasionally, whereas between November and February both configurations undergo deep and repeated discharge cycles. The difference in resilience between the two configurations is clearly visible during these winter months. The state of charge of Scenario B reaches zero far more often than that of Scenario A, and each of these moments marks a day on which the store is empty and the plant must draw the missing energy from the grid. The larger store of Scenario A, by contrast, only rarely runs completely dry, and for most of the winter it retains a reserve that carries the district through the shorter cloudy spells without external support.

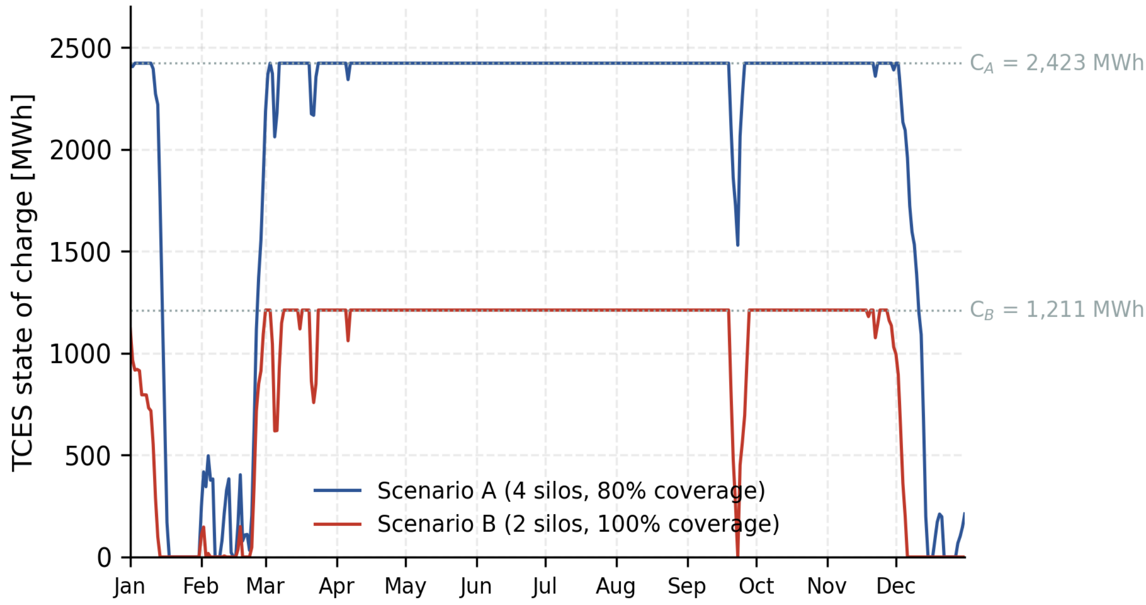

Figure 5.5 TCES state of charge over the reference year for the two scenarios.

5.2.2 Seasonal distribution of the grid imports

Figure 5.6 and Table 5.4 show the monthly distribution of the imports. In both scenarios the grid dependence is entirely concentrated in the December–February period: from March onwards the clear-sky margin designed in Section 3.7 is sufficient to keep the silos charged even through cloudy spells. January is the critical month, with 7.9 GWh imported in Scenario B against 3.3 GWh in Scenario A.

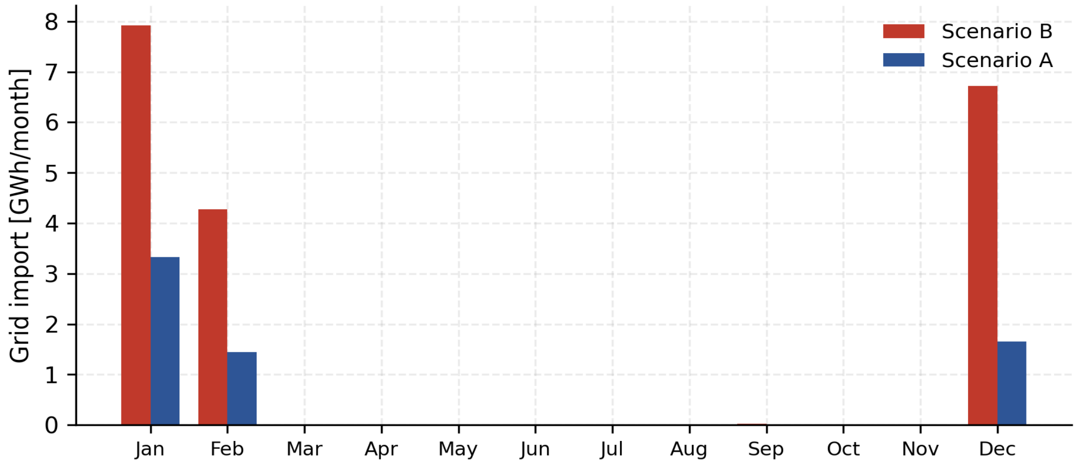

Figure 5.6 Monthly grid import for the two scenarios.

Month	Scenario A [MWh]	Scenario B [MWh]
December	1,657	6,725
January	3,328	7,925
February	1,440	4,277

Month	Scenario A [MWh]	Scenario B [MWh]
March–November	0	19
Year	6,425	18,947

Table 5.4

The winter detail of Figure 5.7 explains the mechanism. In the first half of December a sequence of overcast days progressively discharges both storages: Scenario B, with two days of autonomy, empties after the second consecutive day of low irradiation and starts importing almost daily; Scenario A resists roughly twice as long and partially recharges during the intermediate clear days, so that only the longest perturbations, such as the storm sequence of early January, force it onto the grid.

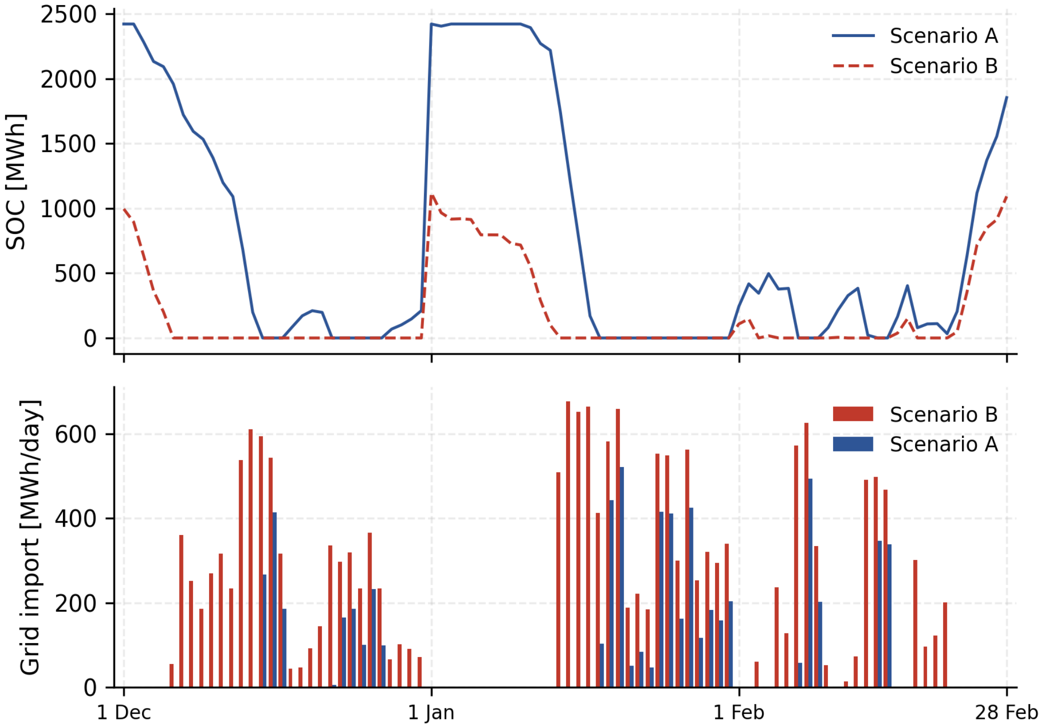

Figure 5.7 Winter: state of charge (top) and daily grid import (bottom) for the two scenarios.

5.2.3 Discussion

The comparison quantifies the trade-off between the two philosophies. Scenario A achieves its quasi-autonomy through a doubled silo dimension, whose economic weight is assessed in Chapter 6, together with the storage-management criterion that lowers the delivered load to 80% on the few critical days, a mild and occasional measure rather than a permanent reduction of service. Scenario B delivers the same full service with half the storage but depends on the grid for about 11% of its winter energy, concentrated in the three winter months, precisely the period in which the electricity system operates under the highest stress and prices.

6) TECHNO-ECONOMIC ANALYSIS

The previous chapters defined and compared the plant configurations on a technical basis: the sizing of the solar field and the storage in Chapter 3, the operational behaviour over the year in Chapter 4, and the comparison between the two storage scenarios and the two power-block layouts in Chapter 5. This chapter completes that comparison on an economic basis, so that the choice of the reference configuration can rest on cost as well as on performance.

The analysis is a preliminary techno-economic assessment: its aim is to estimate the order of magnitude of the investment and to rank the alternatives. It proceeds in the following steps. Section 6.1 defines the economic parameters and the methodology. Section 6.2 builds up the capital cost (CAPEX) component by component, and Section 6.3 estimates the operating cost (OPEX). Section 6.4 combines them into the levelised cost indicators, which are then tested against the uncertainty of the main cost drivers in Section 6.5. Section 6.6 draws the economic comparison together and identifies the reference configuration.

6.1) Economic assumptions and methodology

The costs are evaluated with the parameters listed in Table 6.1. A plant lifetime of 30 years is assumed, consistent with the expected service life of the solar field and of the storage vessels; the $CaO/Ca(OH)_2$ material, being chemically stable and cheap to replenish, does not constrain the plant life. A real discount rate of 5% is adopted, at the lower end of the range commonly used for concentrating-solar studies, reflecting the capital-intensive and low-operating-cost nature of the plant. All costs are referred to the base year 2024; figures originally published in US dollars are converted at 0.92 €/$.

Parameter	Symbol	Value
Plant lifetime	N	30 years
Real discount rate	r	5%
Base year for costs	—	2024
Currency conversion	—	0.92 €/$
Capital recovery factor	CRF	0.06505

Table 6.1

The system boundary coincides with the plant boundary adopted throughout the thesis: the solar island (heliostat field, tower and receiver), the thermochemical storage subsystem (reactors, silos, solids handling and material inventory) and the trigeneration

block (turbines, steam generator, absorption chiller and the plant-side district-heating interface). The district-heating distribution network, the buried piping connecting the plant to the 13,000 apartments, is excluded.
The investment is annualised through the capital recovery factor, which converts the total CAPEX into an equivalent constant annual payment over the plant lifetime:

$$\boldsymbol{CRF} = \frac{\boldsymbol{r}\,(\mathbf{1}+\boldsymbol{r})^{\boldsymbol{N}}}{(\mathbf{1}+\boldsymbol{r})^{\boldsymbol{N}}-\mathbf{1}} = \frac{\mathbf{0.05}\,(\mathbf{1.05})^{\mathbf{30}}}{(\mathbf{1.05})^{\mathbf{30}}-\mathbf{1}} = \mathbf{0.06505\ yr^{-1}}$$

The cost structure is organized to keep two conceptually distinct quantities separate. The first is the industrial cost of running the plant, which comprises the annualized capital and the fixed and variable operating costs of the plant: labor, maintenance, insurance, material make-up, water and auxiliary electricity. The energy exchanged with the grid does not belong to this category: the winter import and the electricity exported by the second turbine are flows between the plant and the external network, not costs of operating the plant, and they are therefore treated separately in the cost-benefit balance of Section 6.6 rather than included in the operating cost. This choice keeps the operating cost of the different configurations comparable independently of how much energy each exchange with the grid. The annualized cost of the plant is thus:

$$C_{ann} = CRF \cdot CAPEX + OPEX$$

where the OPEX contains only the industrial operating items. From this cost the levelized cost of energy (LCOE) is derived, defined as the annualized cost divided by the total useful energy the plant produces, the electricity, heat and cooling delivered to the district and, in the dual-turbine configuration, the electricity exported:

$$LCOE = \frac{C_{ann}}{E_{prod}}$$

The overall economic performance of the plant is then assessed in Section 6.6 through a cash-flow balance, in which the benefits, the avoided cost of the energy supplied to the district and the revenue from the exported electricity, are compared with the costs, including the grid import, to obtain the net present value over the plant life. This is the stage at which the import and the export enter the analysis, on the two opposite sides of the balance.
Finally, a note on the cost data. The unit costs used in Section 6.2 are drawn from public, authoritative sources for the commercial components: the solar field, tower, receiver, power block and steam generator rely on NREL cost models and on the 2024 Annual Technology Baseline. For the components specific to the thermochemical storage, in particular the reactors and the insulated silos, no commercial reference exists at this

scale; the values adopted are order-of-magnitude estimates based on the $CaO/Ca(OH)_2$ research literature. This uncertainty is quantified in the scenario analysis of Section 6.5.

6.2 Capital expenditure (CAPEX)

The capital cost is built up component by component: for each item the total cost is obtained as the product of a specific (unit) cost, taken from specific sources, and the physical size of the component, taken from the sizing of Chapters 3-5. The components are grouped into the three functional blocks of the plant: the solar island, the thermochemical storage and the trigeneration block, and the build-up is carried out for the three configurations compared in Chapter 5:
Scenario A: four silo modules (five-day autonomy at 80% coverage), single turbine;
Scenario A + T2: the same storage, with the second condensing turbine added for surplus recovery;
Scenario B: two silo modules (two-day autonomy at 100% coverage), single turbine.
The three configurations share the same solar island and the same base trigeneration block; they differ only in the two items that depend on the configuration, namely the storage (silos, solids handling and material inventory, which scale with the number of modules) and the power block (the second turbine and its condenser, present only in the dual-turbine layout). Table 6.2 collects the build-up.

Component	Specific cost	Scenario A	Scenario A + T2	Scenario B
CSP — Solar island				
Heliostat field	110 €/m^2	28.3	28.3	28.3
Site improvements	14 €/m^2	3.6	3.6	3.6
Tower (~150 m)	lump	12.0	12.0	12.0
Receiver	180 €/kWth	20.8	20.8	20.8
TCES — Thermochemical storage				
Dehydration reactor (charge)	180 €/kWth	20.7	20.7	20.7
Hydration reactor (discharge)	200 €/kWth	4.0	4.0	5.0
Storage silos (steel, insulated)	180 €/m^3	6.9	6.9	3.4
Solids handling	30 €/m^3	1.1	1.1	0.6
CaO inventory	150 €/t	0.9	0.9	0.4
$Ca(OH)_2$ inventory	200 €/t	1.6	1.6	0.8
Steam management	lump	1.5	1.5	1.5
Trigeneration — Power & thermal block				
Turbine T1 + generator (extraction)	1,330 €/kWe	13.3	13.3	13.3
Steam generator + heat exchangers	180 €/kWth	5.0	5.0	5.0
Turbine T2 + generator (condensing)	1,200 €/kWe	—	12.0	—
Condenser + evaporative tower (T2)	80 €/kWth	—	1.4	—
Absorption chiller	200 €/kW_cold	2.7	2.7	2.7
District-heating interface (plant side)	lump	2.0	2.0	2.0
Direct cost		124.4	137.8	120.1
EPC / indirect (13%)		16.2	17.9	15.6

Contingency (10%)		12.4	13.8	12.0
TOTAL CAPEX		153.0	169.5	147.8

Table 6.2 CAPEX build-up of the three configurations [M€].

6.2.1 Configuration-dependent items

Only two groups of items change across the three configurations. The first is the storage: passing from four modules (Scenario A) to two (Scenario B) halves the silo volume, the solids-handling equipment and the material inventory, for a combined saving of about 5.2 M€. This is a modest figure on the plant scale, and it reflects a distinctive feature of the $CaO/Ca(OH)_2$ system already noted in Chapter 5: the storage material is inexpensive and the silos are simple steel vessels, so that doubling the autonomy adds little to the capital cost. The discharge reactor also differs slightly, being sized on the served winter demand, which is higher in Scenario B where 100% of the load is covered. The second group is the second turbine: in the dual-turbine configuration the condensing group and its dedicated condenser add 13.4 M€ of direct cost, essentially doubling the power-block investment.

6.2.2 Cost structure

The total capital cost is close to 148–153 M€ for the two single-turbine configurations and rises to 170 M€ with the second turbine. The distribution of the direct cost among the three blocks is shown in Figure 6.1 for Scenario A: the solar island is by far the largest block, at about 52% of the direct cost, as expected for a solar-driven plant with a high solar multiple; the storage and the trigeneration blocks account for the remaining 30% and 18% respectively. The breakdown is almost identical in Scenario B, since the storage saving is small; in the dual-turbine configuration the trigeneration share rises to about 27% at the expense of the other two.

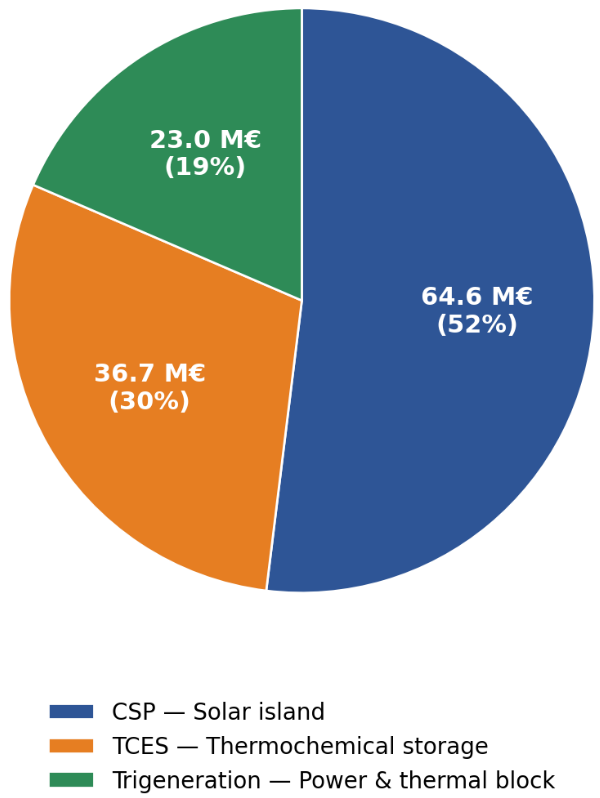

Figure 6.1 Distribution of the direct capital cost among the three plant blocks (Scenario A).

The component-level detail of Figure 6.2 identifies the individual cost drivers. Three items dominate the investment, each of comparable weight: the heliostat field (28.3 M€), the receiver (20.8 M€) and the dehydration reactor (20.7 M€). The prominence of the charge reactor deserves a comment, since it is not obvious a priori. Within the storage block the dominant item is neither the silos nor the material, which together account for about 9 M€ out of 36.7 M€, but the dehydration (charge) reactor. The reason is physical: the charge reactor must absorb the full receiver power of 115 MWth during the hours of peak sun, whereas the discharge reactor is sized on the much lower demand power of about 20-25 MWth; the charging duty therefore drives the reactor cost. This confirms, on an economic level, an argument recurring throughout the thesis: in the $CaO/Ca(OH)_2$ system the expensive element is the power-handling equipment, not the stored energy. The material inventory, calcium oxide and calcium hydroxide together, represents about 1.6% of the total CAPEX, an order of magnitude below what a sensible-heat or electrochemical store of comparable capacity would require.

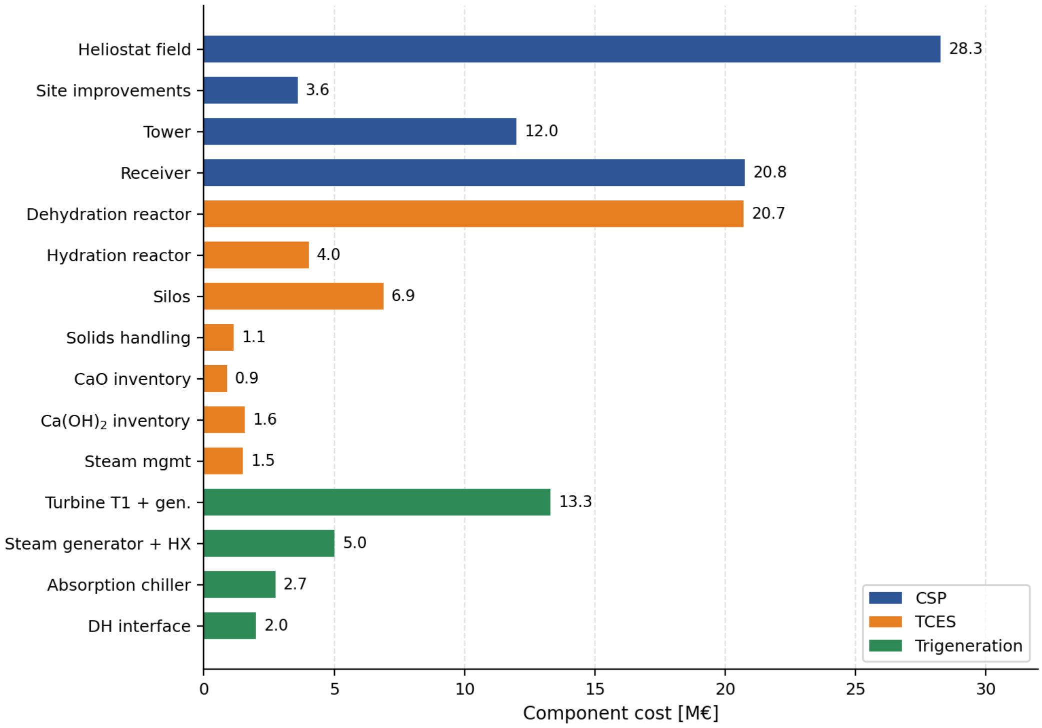

Figure 6.2 Component-level breakdown of the direct capital cost (Scenario A), grouped by functional block.

6.3) Operating expenditure (OPEX)

The annual operating cost gathers the recurring expenses required to run the plant, excluding the annualised capital already treated in Section 6.2. In this section the OPEX is restricted to the industrial operating cost of the plant proper. The energy exchanged with the grid — the winter import and the electricity exported by the second turbine — is not an operating cost of the plant but a flow towards or from the external network; both are therefore treated together in the cost-benefit balance of Section 6.6, and are deliberately left out of the OPEX defined here. This keeps the operating cost of the three configurations comparable on a like-for-like basis, independent of how much energy each one exchanges with the grid.

Item	Basis	Scenario A	Scenario A + T2	Scenario B
Labour personnel	1.0% of CAPEX	1.53	1.70	1.48
Maintenance & spares	0.8% of CAPEX	1.22	1.36	1.18
Insurance & administration	0.2% of CAPEX	0.31	0.34	0.30
Calcium material make-up	10%/yr of CaO inventory	0.09	0.09	0.05
Process water	tariff × demand	0.06	0.06	0.06
Auxiliary electricity	3% of gross generation	0.14	0.14	0.14
TOTAL OPEX		3.35	3.68	3.20

Table 6.3

The first three items, labour, maintenance and insurance, are the operation and maintenance costs, estimated as a percentage of the total capital cost following the standard practice for concentrating-solar plants. Their sum, equal to 2% of the CAPEX per year, is dominated by maintenance and spare parts, which reflects the cleaning of the heliostat field, the servicing of the solids-handling equipment and the periodic overhaul of the turbines. Being proportional to the investment, these items are highest for the dual-turbine configuration and lowest for Scenario B, mirroring the ranking of the capital costs.

The calcium material make-up accounts for the gradual loss of storage capacity caused by the cyclic degradation of the storage material. The make-up therefore applies to the calcium material as a whole and is counted only once, referred to the CaO mass; it represents the loss of reactivity (sintering, incomplete conversion) that accumulates over repeated cycles. A conservative rate of 10% per year is assumed, yet because the material is inexpensive the resulting cost stays below 0.09 M€/yr, a further confirmation that the low material cost is a structural advantage of the $CaO/Ca(OH)_2$ system.

The process water covers the losses of the water that circulates in a closed loop between the two reactors: in principle the water released on charging is entirely reabsorbed on discharging, so only the minor make-up for purges, entrainment and evaporation is charged here.

The auxiliary electricity accounts for the parasitic loads of the plant, the electricity the plant consumes to operate itself rather than the electricity it produces. The main contributions are the heliostat tracking drives, which continuously orient the large mirror field, the pumps of the steam and cooling circuits, and the solids-handling equipment (elevators and conveyors) that moves the material between reactors and silos. These loads are estimated at 3% of the gross electricity generation and valued at the self-consumption price, giving about 0.14 M€/yr.

6.3.1 Cost structure

Figure 6.3 shows the composition of the annual OPEX for the three configurations. Two features stand out. First, the operating cost is strongly dominated by the fixed O&M items labour, maintenance and insurance together account for about 92% of the total, a direct consequence of the plant having no fuel cost and of the grid import being excluded from this boundary. Second, the three configurations differ very little: the two Scenario A layouts are marginally higher because of their larger material inventories, but the operating cost is essentially decoupled from the storage size. Running the plant costs almost the same regardless of the number of silos; the real economic distinction between the scenarios emerges only once the grid exchanges are accounted for, in Section 6.6.

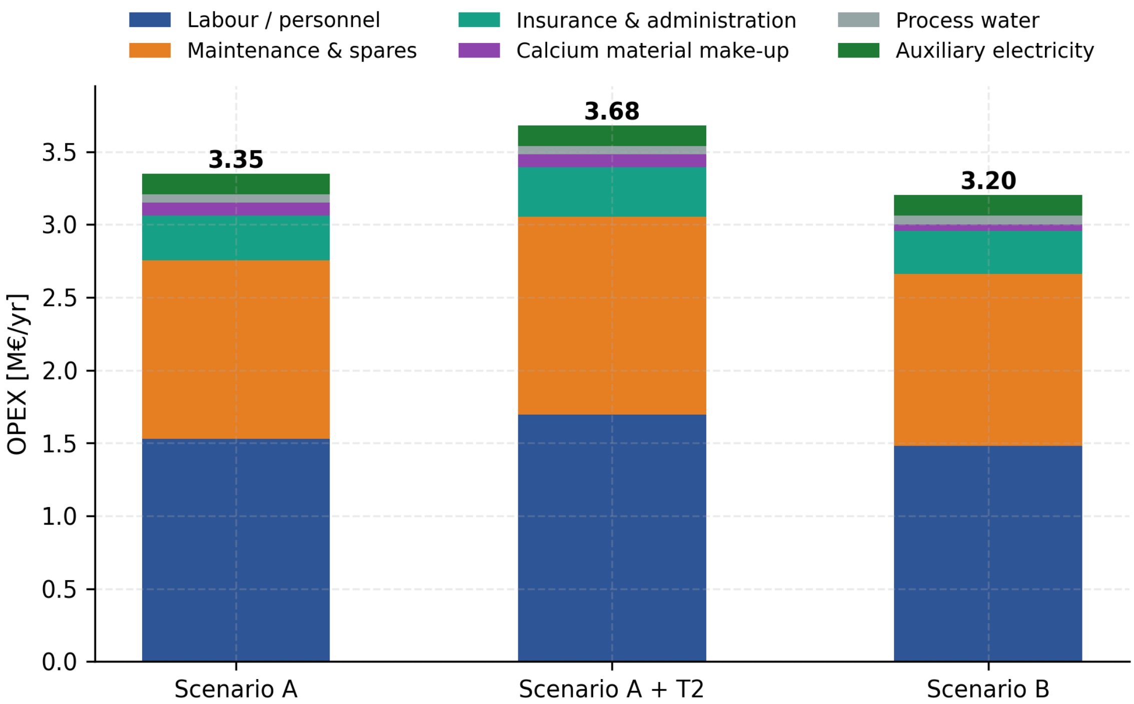

Figure 6.3 Composition of the annual OPEX for the three configurations

Figure 6.4 details the individual weight of each item for the reference dual-turbine configuration. Maintenance and labour alone make up more than four fifths of the operating cost, while the three process-related items, material make-up, water and auxiliary electricity, together account for less than one tenth, with the calcium make-up, the item most specific to a thermochemical storage plant, contributing only about 2% of the total.

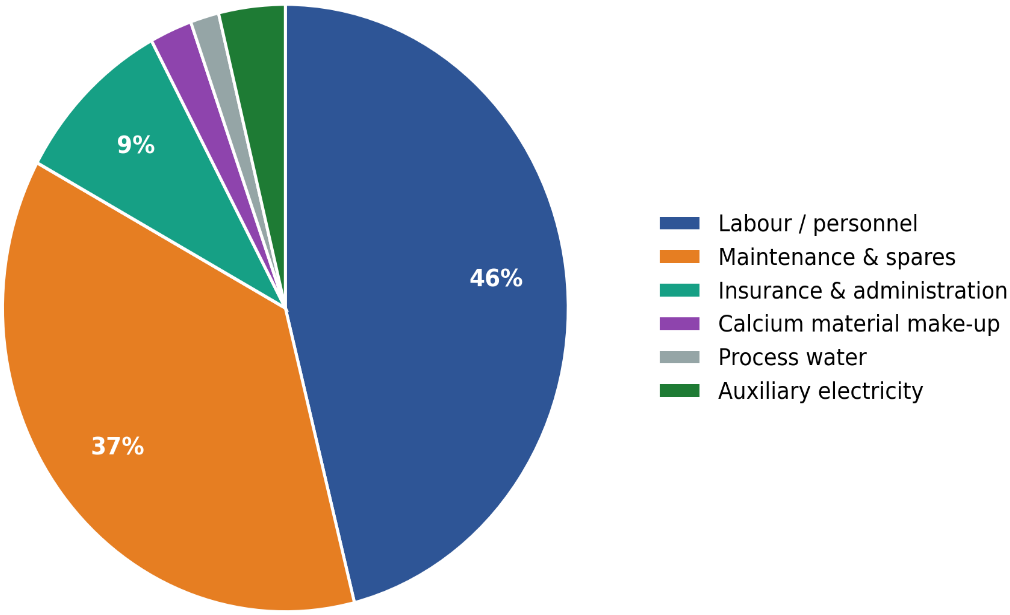

Figure 6.4 Detailed breakdown of the annual OPEX for the Scenario A + T2 configuration.

6.4) Economic balance and cash-flow analysis

The capital and operating costs of the previous sections describe what the plant costs; this section quantifies what it is worth. To do so, the yearly cash flow of the plant is built over its 30-year life, comparing the costs it incurs with the benefits it generates, and discounting both to the present to obtain the net present value (NPV) of the investment. The analysis is carried out for the three configurations, so that the choice between them can rest on a complete economic picture.

6.4.1 Valuation of the benefits

The plant delivers four energy services to the district, electricity, space heating, domestic hot water and cooling and in the dual-turbine configuration, exports electricity to the grid. Each of these flows is assigned an economic value.

The four services are valued at the price the district would otherwise pay to obtain them from the market: the benefit of the plant is the avoided expenditure of its 32,500 inhabitants. The reference prices are the Spanish household tariffs for 2024, taken from Eurostat, and are collected in Table 6.4. The electricity delivered is valued at the household retail price of 240 €/MWh, which includes the energy, network and tax components actually paid by a domestic consumer. Space heating and domestic hot water, which would otherwise be produced by gas boilers, are valued at the household natural-gas price of 90 €/MWh. The cooling service is valued at 70 €/MWh of cold delivered, corresponding to the electricity that an equivalent electric chiller would consume to provide the same cooling. These prices are applied to the full annual demand of each service, the district receives essentially all of its energy in every configuration.

Service	Annual energy	Unit value	Source	Annual benefit
Electricity	39,000 MWh	240 €/MWh	Eurostat, ES household 2024	9.36 M€
Space heating	39,000 MWh	90 €/MWh	Eurostat, ES gas 2024	3.51 M€
Domestic hot water	19,500 MWh	90 €/MWh	Eurostat, ES gas 2024	1.75 M€
Cooling (cold delivered)	28,700 MWh	70 €/MWh	electricity for equiv. chiller	2.01 M€
T2 export (A+T2 only)	43,600 MWh	90 €/MWh	ES wholesale, night-shifted	3.92 M€

Table 6.4

The electricity exported by the second turbine is valued differently at 90 €/MWh. This is lower than the retail price at which imported electricity is valued, and the asymmetry is physical: when the plant buys from the grid it pays the full retail price, energy, network charges and taxes, when it sells, only the energy component is remunerated, since the network and fiscal components are borne by the final consumer of that electricity. The export price is nevertheless set above the pure solar-capture price, because the storage allows the second turbine to dispatch part of its output in the evening and night hours, when wholesale prices are higher, rather than only at the midday solar peak.

The resulting annual benefits are shown in Figure 6.5 for the dual-turbine configuration. The avoided electricity cost is by far the largest single item, a direct consequence of the high retail value of electricity; the export revenue, present only in this configuration, is comparable to the avoided heating cost.

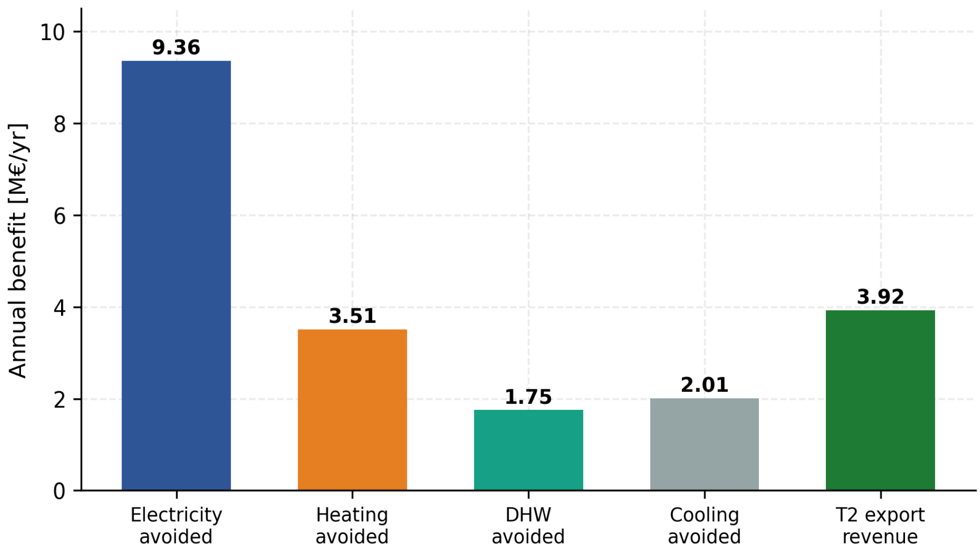

Figure 6.5 Composition of the annual benefits for the Scenario A + T2 configuration.

6.4.2 Financial parameters and method

The costs entering the balance are the plant OPEX of Section 6.3 and the cost of the winter grid import, valued at the import price of 100 €/MWh; both the import and the export are treated here, as the flows exchanged with the grid, rather than in the OPEX. The initial investment is the CAPEX of Section 6.2, incurred at year zero.
Future cash flows are discounted with the real discount rate of 5% adopted in Section 6.1, which reflects the long-lived, capital-intensive nature of the plant. The net present value after N years is the sum of the discounted annual cash flows net of the initial investment:

$$NPV = -CAPEX + \sum_{t=1}^{N} \frac{B - C}{(1+r)^t}$$

where B is the annual benefit and C the annual cost. The discounted payback time is the year in which the cumulative NPV first becomes positive, and the levelised cost of energy (LCOE) is the ratio of the annualised total cost to the energy produced.

6.4.3 Results

Table 6.5 summarises the outcome for the three configurations, and Figure 6.6 traces the cumulative NPV over the plant life.

Indicator	Scenario A	Scenario A + T2	Scenario B
CAPEX	153.0 M€	169.5 M€	147.8 M€
Annual benefit	16.63 M€	20.56 M€	16.63 M€
Annual cost (OPEX + import)	3.99 M€	4.32 M€	5.10 M€
Net annual cash flow	12.64 M€	16.24 M€	11.54 M€
NPV at 30 years	+41.3 M€	+80.1 M€	+29.6 M€
Discounted payback	20 yr	16 yr	21 yr
LCOE	105 €/MWh	87 €/MWh	102 €/MWh

Table 6.5

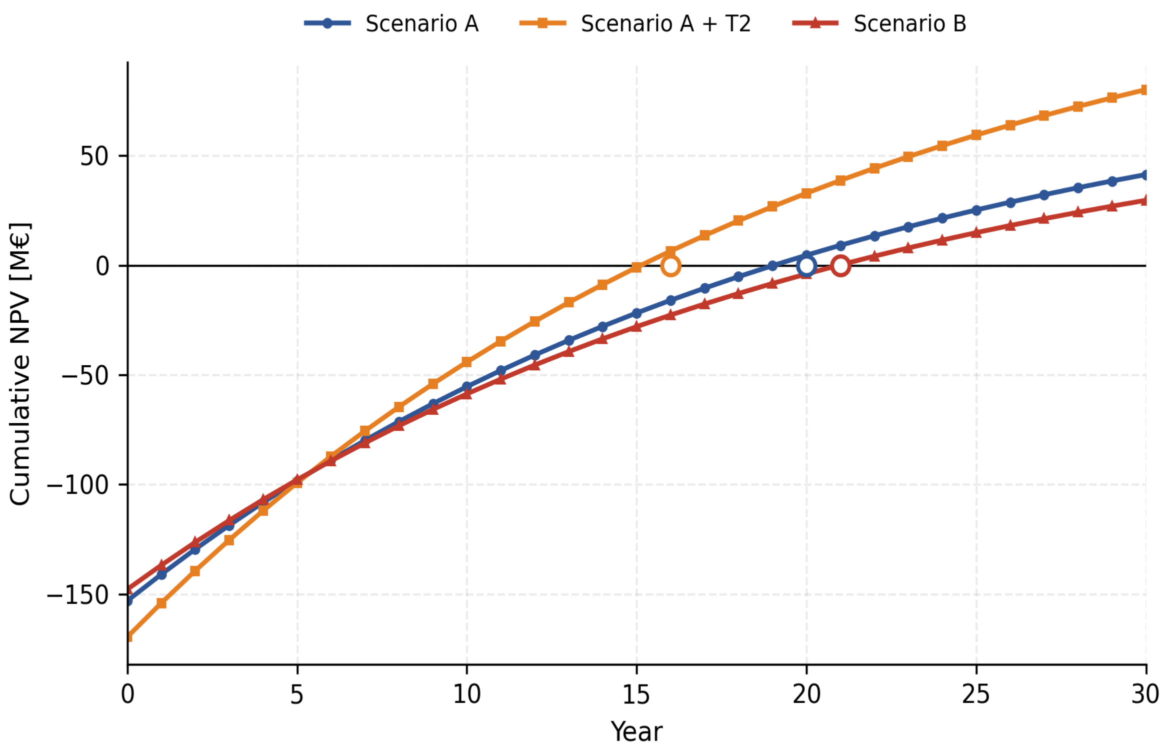

Figure 6.6 Cumulative net present value of the three configurations over the 30-year plant life

All three configurations reach a positive NPV within the plant life, so the plant is a sound investment in every case; but the ranking is clear. The dual-turbine configuration is markedly the best, with an NPV of 80 M€ and a payback of 16 years, roughly double the NPV of the other two. Its advantage comes entirely from the export revenue: the second turbine converts into 3.9 M€/yr of income the surplus solar energy that would otherwise be defocused, at the cost of a modest increase in CAPEX and OPEX. The economic result thus confirms, on financial grounds, the technical case made for the second turbine in Chapter 5.

Between the two single-turbine options, Scenario A slightly outperforms Scenario B (NPV 41 vs 30 M€) despite its higher capital cost. The reason lies in the operating balance: the larger storage of Scenario A reduces the winter grid import to 6.4 GWh/yr, against 18.9 GWh/yr for Scenario B, and this lower import cost more than compensates the additional investment in silos over the plant life. The reduced autonomy of Scenario B, cheaper to build, turns out to be more expensive to run.
The LCOE tells the same story from the cost side. The dual-turbine configuration achieves the lowest levelised cost, 87 €/MWh, because it spreads a similar total cost over a larger energy output, the district services plus the exported electricity. The two single-turbine configurations sit around 102-105 €/MWh. All three values are competitive with the levelised cost of dispatchable low-carbon generation, which is a notable result for a plant that delivers firm, storable renewable heat and power to a residential district without fossil back-up.

6.4.4 Sensitivity to the reference prices

The benefits, and hence the NPV, depend on the assumed energy prices, which are the most uncertain inputs of the analysis. The electricity retail price is the dominant driver, since avoided electricity is the largest benefit: a variation of ±20% in this price alone shifts the annual benefit by about ±1.9 M€ and the 30-year NPV by roughly ±30 M€. The results should therefore be read as representative of the 2024 Spanish price context; a sustained period of lower energy prices would lengthen the payback, while the current environment of high and volatile prices reinforces the economic case for a plant that shields the district from that volatility. This price dependence, rather than the plant cost, is the true determinant of the investment's profitability.

6.5) Economic scenarios

The net present values obtained in Section 6.4 rest on a set of assumptions, component costs, energy prices, discount rate, that are known only approximately. Some of them, in particular the cost of the thermochemical reactors, are order-of-magnitude estimates for a technology that is not yet commercial; others, such as the retail price of electricity, are subject to considerable market volatility. A single point value of the NPV would therefore give a false impression of precision. This section replaces it with a range, by defining three combined scenarios, worst, actual and best and recomputing the economic indicators of all three plant configurations under each.

6.5.1 Definition of the scenarios

Five parameters are identified as the most uncertain and, at the same time, the most influential on the result. Two are on the cost side: the specific cost of the reactors, the least established item of the CAPEX, and the cost of the heliostat field, the largest single component. Two are on the revenue side: the retail electricity price, which governs the

dominant benefit, and the export price of the electricity sold to the grid. The last is the real discount rate, which sets the weight of the future cash flows against the initial investment.
The three scenarios are built by moving these parameters together towards the unfavourable or the favourable end of their plausible range. The worst scenario combines high costs, low energy prices and a high discount rate; the best scenario combines the opposite; the actual scenario is the reference case of Section 6.4. The bounds of the worst scenario are kept realistic rather than catastrophic — a plausible adverse combination, not the simultaneous extreme of every driver — so that the resulting range represents a credible span of outcomes.

Parameter	Unit	Worst	Actual	Best
Reactor cost	€/kWth	300	200	100
Heliostat cost	€/m^2	150	110	90
Electricity price	€/MWh	200	240	280
Export price	€/MWh	60	90	110
Discount rate	%	6	5	4

Table 6.6

6.5.2 Results

Table 6.7 and Figure 6.7 report the 30-year NPV of the three configurations in the three scenarios, and Figure 6.8 the corresponding levelised cost of energy.

Configuration	Worst	Actual	Best
Scenario A — NPV [M€]	−38.2	+37.6	+116.3
Scenario A — payback [yr]	> 30	20	12
Scenario A + T2 — NPV [M€]	−23.3	+76.4	+177.0
Scenario A + T2 — payback [yr]	> 30	16	10
Scenario B — NPV [M€]	−48.2	+25.9	+102.5
Scenario B — payback [yr]	> 30	22	13
A + T2 — LCOE [€/MWh]	110	88	71

Table 6.7

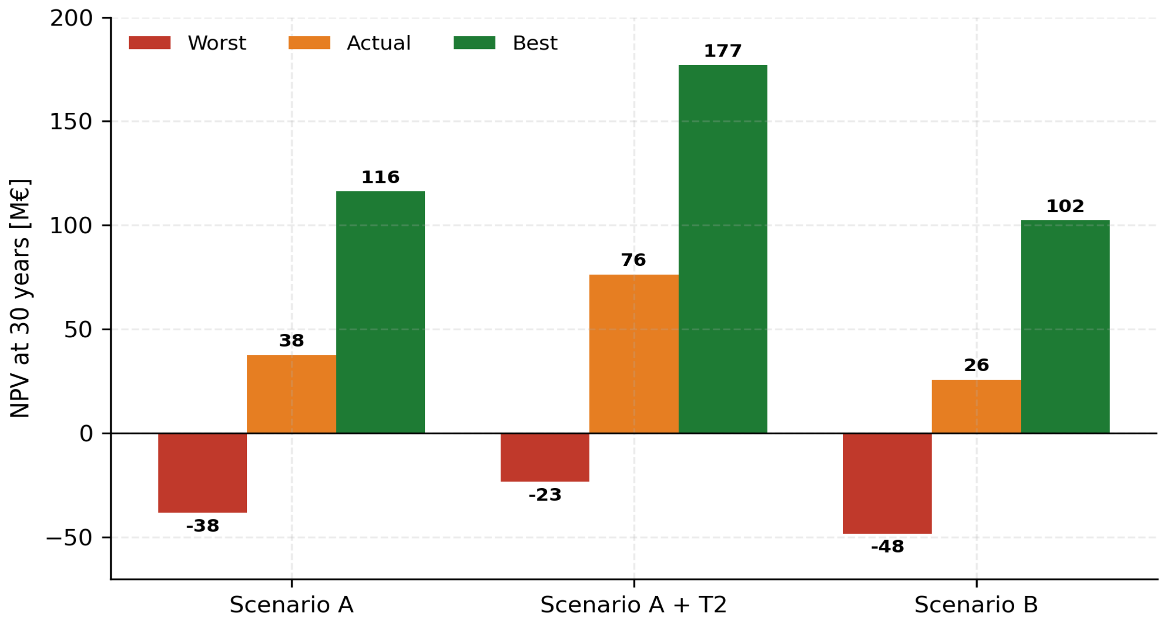

Figure 6.7 Net present value at 30 years for the three configurations under the worst, actual and best scenarios.

Three conclusions emerge from the analysis:

First, in the central case all three configurations are profitable, and in the favourable case markedly so: the dual-turbine plant reaches an NPV of 177 M€ and a payback of ten years when costs are low and energy prices high. The upside potential of the investment is therefore considerable, and directly linked to the energy-price environment.

Second, even in the adverse scenario the losses are contained. The worst-case NPV of the dual-turbine configuration is −23 M€ on an investment of about 170 M€, a shortfall of the order of 15% of the capital, rather than the collapse that an all-extreme combination would suggest. The plant does not pay back within its life in this scenario, but it recovers the large majority of its investment even under a simultaneous deterioration of costs, prices and the cost of capital. The break-even is close, which means that a comparatively small improvement in any of the drivers, a slightly higher electricity price, a lower reactor cost, is enough to bring the plant back into profit.
Third, and most importantly for the design choice, the ranking of the configurations is completely stable across the whole range. In every scenario the dual-turbine configuration is the best and Scenario B the worst, with the single-turbine Scenario A in between. The advantage of A+T2 over the next-best option is 30 to 60 M€ depending on the scenario, and it is the configuration that stays closest to break-even in the worst case and rises highest in the best. Whatever the future values of costs and prices turn out to be, the choice of adding the second turbine is therefore economically robust: the decision does not hinge on the particular assumptions of the reference case.

6.5.3 Discussion

Among the five drivers, the two that move the result most are the electricity price and the reactor cost. The electricity price acts on the largest benefit, the avoided cost of the electricity delivered to the district, and therefore drives the revenue side; the reactor cost acts on the most uncertain and one of the largest CAPEX items, and therefore drives the cost side. The heliostat cost, the export price and the discount rate play a secondary role. This is visible also in the levelised cost of Figure 6.8: the LCOE of the dual-turbine configuration ranges from 71 €/MWh in the best case to 110 €/MWh in the worst, always the lowest of the three configurations because the same cost base is spread over the larger energy output that includes the exported electricity.

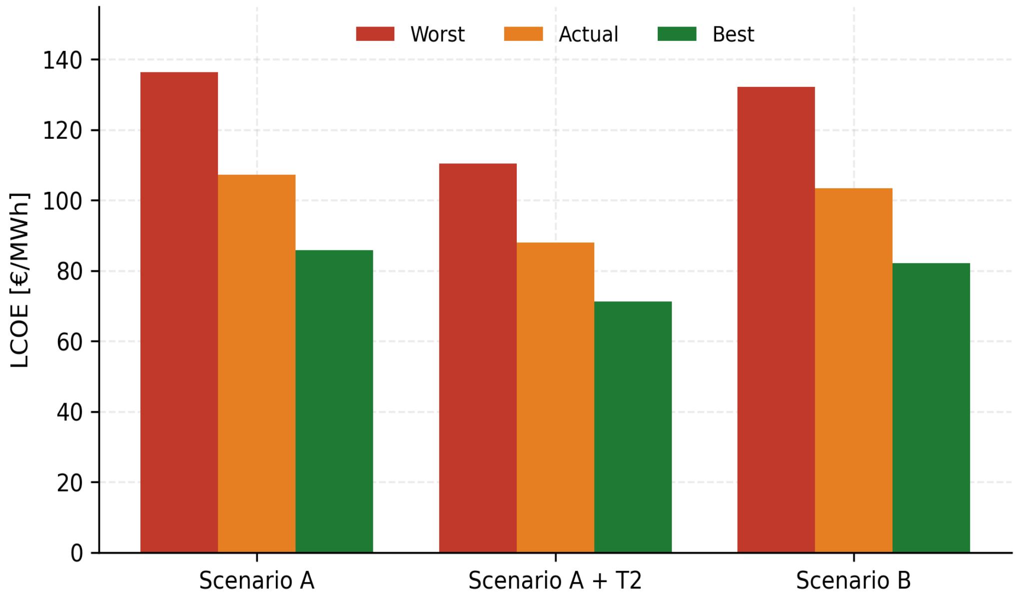

Figure 6.8 Levelised cost of energy for the three configurations under the three scenarios.

The overall message is that the plant is a sound investment under central and favourable conditions, and a contained risk under adverse ones, with the return conditioned mainly by the price of electricity and the cost of the reactor technology. As these two drivers improve, the first with the current trend of electricity prices, the second with the expected maturing of thermochemical-storage technology, the economic case can only strengthen. In all cases the internal comparison between the configurations is unaffected, and the technical preference for the surplus-recovering second turbine established in Chapter 5 is confirmed as the economically soundest choice.

6.6) Reference configuration and concluding remarks

The technical analysis of Chapter 5 and the economic analysis of this chapter can now be brought together to identify the reference configuration of the plant. The three options compared throughout, Scenario A with a single turbine, the same storage with the surplus-recovering second turbine (A + T2), and the reduced-storage Scenario B, have been evaluated on their operation over the year, their capital and operating costs, their net present value and their robustness to uncertain assumptions. Every one of these criteria points to the same choice.

6.6.1 Synthesis of the comparison

Table 6.8 collects the main indicators of the three configurations under the reference assumptions.

Indicator	Scenario A	Scenario A + T2	Scenario B
Storage autonomy	5 days	5 days	2 days
Silo modules	12	12	7
Defocused energy	125.8 GWh/yr	4.5 GWh/yr	102.5 GWh/yr
Electricity export	—	43.6 GWh/yr	—
Grid import	6.4 GWh/yr	6.4 GWh/yr	18.9 GWh/yr
CAPEX	153.0 M€	169.5 M€	147.8 M€
OPEX	3.35 M€/yr	3.68 M€/yr	3.20 M€/yr
Annual benefit	16.63 M€/yr	20.56 M€/yr	16.63 M€/yr
NPV at 30 years	+41.3 M€	+80.1 M€	+29.6 M€
Discounted payback	20 yr	16 yr	21 yr
LCOE	105 €/MWh	87 €/MWh	102 €/MWh

Table 6.8

The picture is consistent across the whole table. Scenario B, cheapest to build, is the least attractive once operation is taken into account: its two-day autonomy forces almost three times the grid import of the other options, so that its lower capital cost is eroded by a higher operating cost over the plant life, leaving it with the lowest NPV and the longest payback. Scenario A corrects this by enlarging the storage to five-day autonomy, which cuts the winter import to a third and lifts the NPV well above Scenario B, but it leaves unsolved the mirror problem identified in Chapter 5, the rejection of almost half of the collected solar energy through defocusing. The dual-turbine configuration closes precisely this gap.

6.6.2 The role of the second turbine

The addition of the second turbine is the single design decision that most improves the plant, and it does so on both the technical and the economic side simultaneously. Technically, it reduces the defocused energy from 125.8 to 4.5 GWh per year, a 96% recovery of what would otherwise be wasted, by converting the summer solar surplus into 43.6 GWh of exported electricity, with the storage acting as a day-and-night buffer that lets the turbine run far beyond the sunlight hours. Economically, that exported electricity is worth 3.9 M€ per year, which raises the annual benefit from 16.6 to 20.6 M€ against a modest increase of 16.5 M€ in capital cost and 0.3 M€/yr in operating cost. The result is an NPV of 80 M€, roughly double that of either single-turbine option, the shortest payback of the three at sixteen years, and the lowest levelised cost at 87 €/MWh, the last because the same cost base is spread over a larger useful output.

Crucially, this advantage is not an artefact of the reference assumptions. The scenario analysis of Section 6.5 showed that the dual-turbine configuration remains the best in every case examined, from the adverse combination of high costs and low prices to the favourable one, with a margin of 30 to 60 M€ over the next-best option throughout. The economic preference for the second turbine is therefore robust, and it coincides with the technical argument developed in Chapter 5: the same feature that makes the plant work better also makes it more profitable.

6.6.3 Reference configuration

On the basis of this convergent evidence, the Scenario A + T2 configuration is adopted as the reference plant of this thesis: a solar field of 256,884 m^2 feeding a 115 MW receiver, a $CaO/Ca(OH)_2$ thermochemical store of twelve silo modules providing five days of autonomy, a first 10 MW extraction turbine serving the trigeneration demand of the district, and a second 10 MW condensing turbine recovering the solar surplus for export. This configuration supplies the full electricity, heating, domestic-hot-water and cooling demand of a district of 13,000 dwellings almost entirely from concentrated solar energy, with only 6.4 GWh of annual grid import as winter backup, while exporting 43.6 GWh of renewable electricity to the grid; and it does so with a positive net present value of 80 M€ and a levelised cost of 87 €/MWh under the reference assumptions.

Two qualifications should accompany this conclusion. The first is that the profitability, though robust in its ranking, is conditioned by the energy-price environment: the plant is highly attractive at current electricity prices and would become marginal only under a sustained fall in those prices, as quantified in Section 6.5. The second is that the cost of the thermochemical reactors, the least established item of the investment, has been treated through a wide range rather than a single figure; a firmer estimate, which only the maturing of the technology can provide, would narrow the uncertainty band around the reference result. Neither qualification alters the central finding of the techno-economic analysis: a CSP plant coupled to $CaO/Ca(OH)_2$ thermochemical storage and a dual-turbine power block can supply firm, storable, low-carbon energy to a residential district at a competitive cost, and the recovery of the solar surplus through a second turbine is the decisive step that makes it both technically effective and economically sound.

7) CONCLUSIONS

This thesis investigated the integration of a $CaO/Ca(OH)_2$ thermochemical energy storage system within a concentrated solar power (CSP) plant designed to supply electricity, heating, domestic hot water and cooling to a residential district in southern Spain. The work addressed the challenge of increasing the dispatchability of renewable energy systems through the combination of solar thermal generation, long-duration energy storage and a trigeneration block, following the complete design chain from the sizing of the components to the annual operational simulation and the techno-economic assessment.

The results indicate that the proposed integration is technically feasible under the assumptions adopted in the study. The thermodynamic characteristics of the $CaO/Ca(OH)_2$ cycle are compatible with the operating conditions of central-receiver CSP systems, allowing solar heat to be stored as chemical potential and later recovered as high-temperature thermal energy. This enables the decoupling between solar energy collection and final energy delivery that is one of the principal requirements of a dispatchable renewable energy system. The sizing methodology developed in this work led to a plant configuration capable of supplying the energy requirements of a district of approximately 13,000 dwellings, and the annual simulations show that the combination of CSP generation and thermochemical storage can greatly reduce the dependence on external energy sources while meeting the electrical and thermal demands during periods of low solar availability. The degree of energy independence achieved remains, however, dependent on the storage capacity selected and on the occurrence of prolonged adverse weather conditions: the five-day quasi-autonomous configuration limits the winter grid import to 6.4 GWh per year but does not eliminate it.

The study also highlights the operational flexibility provided by the proposed storage architecture. The possibility of delivering heat either directly to the thermal users or indirectly through electricity production allows the plant to respond to demand profiles that vary widely through the year, and this flexibility proved particularly relevant in winter, when the thermal and electrical demands reach their highest levels simultaneously.

A significant outcome of the operational analysis concerns the seasonal imbalance between solar production and user demand. While the storage mitigates the short-term and multi-day mismatches, a substantial solar surplus remains available during the periods of high irradiance, and in the single-turbine configuration a considerable fraction of it, almost half of the collected energy, would be curtailed. The addition of a second condensing turbine provides an effective strategy for recovering this otherwise unused energy through electricity export, reducing the annual curtailment by 96%.

From an economic perspective, the results suggest that the configuration including the additional turbine offers clear advantages under the reference assumptions, reaching a net present value of about 80 M€ over the plant life and a levelized cost of energy of 87 €/MWh. Nevertheless, the economic performance remains sensitive to several parameters, particularly the electricity price, the discount rate and the capital cost of the thermochemical storage equipment; the sensitivity analysis shows that these factors have a substantial influence on the profitability and should be carefully considered in the evaluation of future industrial implementations. An important observation emerging from the cost structure is that the storage material itself represents only a limited fraction of the total investment, while the main economic burden is associated with the reactors and the other power-handling equipment. This feature distinguishes thermochemical storage from several alternative technologies and is advantageous for applications requiring extended storage durations, although further research is needed to validate the cost estimates at commercial scale.

The environmental characteristics of the $CaO/Ca(OH)_2$ cycle also deserve consideration. The storage materials are abundant, widely available and non-toxic, which facilitates large-scale deployment, reduces the concerns related to critical raw materials and allows the plant to be sited close to the district it serves. At the same time, the practical implementation of the technology still faces challenges associated with the reactor design, the handling of large solid flows, the degradation of the material over repeated cycles and the long-term operational reliability. The conclusions of this study must be interpreted in light of these limitations: the reactor performance was represented through equilibrium-based models, with kinetic effects and degradation mechanisms incorporated only through simplified coefficients, and some cost estimates rely on data extrapolated from pilot-scale systems, since large commercial installations based on the $CaO/Ca(OH)_2$ cycle do not yet exist. Further experimental validation and scale-up studies will therefore be necessary to reduce the uncertainties and confirm the performance predicted by the present work.

Overall, the study indicates that the integration of CSP technology with $CaO/Ca(OH)_2$ thermochemical storage represents a viable approach for long-duration renewable energy storage and district-scale trigeneration. Although significant technological and economic uncertainties remain, the results suggest that this concept deserves further investigation as a concrete contribution to future low-carbon and dispatchable energy systems.

References

[1] A. J. Aguilar, M. L. de la Hoz-Torres, J. Aguilar-Camacho, and M. F. Guerrero-Rivera, "Assessment of Energy Efficiency and Energy Poverty of the Residential Building Stock of the City of Seville Using GIS," *Applied Sciences*, vol. 15, no. 12, art. no. 6438, 2025, doi: 10.3390/app15126438.

[2] K. Wang, T. Yan, R. K. Li, and W. G. Pan, "A review for $Ca(OH)_2/CaO$ thermochemical energy storage systems," *Journal of Energy Storage*, vol. 50, art. no. 104612, 2022, doi: 10.1016/j.est.2022.104612.

[3] Y. Jia, Y. Wang, X. Zhou, Y. Xu, M. Liu, H. Ling, and H. Chen, "Critical review of $CaO/Ca(OH)_2$ thermochemical energy storage material," *Renewable and Sustainable Energy Reviews*, vol. 216, art. no. 115678, 2025, doi: 10.1016/j.rser.2025.115678.

[4] M. Schmidt, C. Szczukowski, C. Roßkopf, M. Linder, and A. Wörner, "Experimental results of a 10 kW high temperature thermochemical storage reactor based on calcium hydroxide," *Applied Thermal Engineering*, vol. 62, no. 2, pp. 553–559, 2014, doi: 10.1016/j.applthermaleng.2013.09.020.

[5] M. Schmidt, M. Gollsch, F. Giger, M. Grün, and M. Linder, "Development of a moving bed pilot plant for thermochemical energy storage with $CaO/Ca(OH)_2$," *AIP Conference Proceedings*, vol. 1734, art. no. 050041, 2016.

[6] M. Schmidt and M. Linder, "Power generation based on the $Ca(OH)_2/CaO$ thermochemical storage system — Experimental investigation of discharge operation modes in lab scale and corresponding conceptual process design," *Applied Energy*, vol. 203, pp. 594–607, 2017, doi: 10.1016/j.apenergy.2017.06.063.

[7] A. Carro, R. Chacartegui, C. Ortiz, and J. A. Becerra, "Analysis of a thermochemical energy storage system based on the reversible $Ca(OH)_2/CaO$ reaction," *Energy*, vol. 261, art. no. 125064, 2022, doi: 10.1016/j.energy.2022.125064.

[8] A. Carro, R. Chacartegui, C. Ortiz, J. Arcenegui-Troya, L. A. Pérez-Maqueda, and J. A. Becerra, "Integration of calcium looping and calcium hydroxide thermochemical systems for energy storage and power production in concentrating solar power plants," *Energy*, vol. 283, art. no. 128388, 2023, doi: 10.1016/j.energy.2023.128388.

[9] A. Carro, R. Chacartegui, C. Ortiz, and J. A. Becerra, "Indirect power cycles integration in concentrated solar power plants with thermochemical energy storage based on calcium hydroxide technology," *Journal of Cleaner Production*, vol. 421, art. no. 138417, 2023, doi: 10.1016/j.jclepro.2023.138417.

[10] J. Arcenegui-Troya, A. Carro, C. Ortiz, R. Chacartegui, A. Perejón, L. A. Pérez-Maqueda, and P. E. Sánchez-Jiménez, "Unlocking synergistic benefits of the calcium looping-calcium hydroxide integration for energy storage: A perspective on sorbent performance," *Chemical Engineering Journal*, vol. 504, art. no. 158775, 2025, doi: 10.1016/j.cej.2024.158775.

[11] H. Liu, Y. Zhang, Q. Xu, W. Han, K. Zhang, X. Yang, C. Yang, S. Li, and J. Shen, "Carnot battery with thermochemical energy storage and supercritical CO_2 power cycle: Thermodynamic and techno-economic characteristics," *The Innovation Energy*, vol. 3, no. 2, art. no. 100163, Apr. 2026, doi: 10.59717/j.xinn-energy.2026.100163.

[12] Siemens Energy, *Efficiency: More Value to Your Facility — Industrial Steam Turbines*, company brochure, Siemens Energy Global GmbH & Co. KG, Görlitz, Germany, 2024. [Online]. Available: https://www.siemens-energy.com/steamturbines

[13] A. Kamel, K. M. S. Khalil, A. Askalany, E. S. Ali, K. Harby, and M. Ghazy, "Improving adsorption materials properties for renewable energy-driven cooling systems," *Thermal Science and Engineering Progress*, vol. 50, art. no. 102551, 2024, doi: 10.1016/j.tsep.2024.102551.

[14] P. Kurup, S. Akar, S. Glynn, C. Augustine, and P. Davenport, *Cost Update: Commercial and Advanced Heliostat Collectors*, National Renewable Energy Laboratory, Golden, CO, USA, Tech. Rep. NREL/TP-7A40-80482, 2022. [Online]. Available: https://www.nrel.gov/docs/fy22osti/80482.pdf

[15] National Renewable Energy Laboratory, "System Advisor Model (SAM) — CSP power tower installation costs," online documentation. [Online]. Available: https://samrepo.nrelcloud.org/help/cc_tower.html [Accessed: Jul. 2026].

[16] National Renewable Energy Laboratory, "Annual Technology Baseline 2024 — Concentrating Solar Power," 2024. [Online]. Available: https://atb.nrel.gov/electricity/2024/concentrating_solar_power [Accessed: Jul. 2026].

[17] Bidragon Machinery, "How to choose the silo size — industrial steel silo sizing and cost guide." [Online]. Available: https://www.bidragonsilo.com/how-to-choose-the-silo-size/ [Accessed: Jul. 2026].

[18] IQS Directory, "Screw conveyors and bulk solid-handling equipment — technical overview." [Online]. Available: https://www.iqsdirectory.com/articles/screw-conveyors.html [Accessed: Jul. 2026].